Long-term potentiation at pyramidal cell to somatostatin interneuron synapses controls hippocampal network plasticity and memory

Azam Asgarihafshejani[1,#], Ève Honoré[1,#], François-Xavier Michon[1], Isabel Laplante[1] and Jean-Claude Lacaille[1,2,*]

[1]Department of Neurosciences, Center for Interdisciplinary Research on Brain and Learning (CIRCA) and Research Group on Neural Signaling and Circuitry (GRSNC), Université de Montréal, Montreal, Quebec, H3C 3J7, Canada.

[2]Lead Contact

[#]Equally contributing authors

*Correspondence: jean-claude.lacaille@umontreal.ca

Total figures and/or tables: Fig 1-4, Fig S1-S4, Table S1

SUMMARY

Hippocampal somatostatin (SOM) cells are dendrite-projecting inhibitory interneurons. CA1 SOM cells receive major excitatory inputs from pyramidal cells (PC-SOM synapses) which show mGluR1a- and mTORC1-mediated long-term potentiation (LTP). PC-SOM synapse LTP contributes to CA1 network metaplasticity and memory consolidation, but whether it is sufficient to regulate these processes remains unknown. Here we used optogenetic stimulation of CA1 pyramidal cells and whole cell recordings in slices to show that optogenetic theta burst stimulation

(TBS_{opto}) produces LTP at PC-SOM synapses. At the network level, we found that TBS_{opto} differentially regulates metaplasticity of pyramidal cell inputs: enhancing LTP at Schaffer collateral synapses and depressing LTP at temporo-ammonic synapses. At the behavioral level, we uncovered that in vivo TBS_{opto} regulates learning-induced LTP at PC-SOM synapses, as well as contextual fear memory. Thus, LTP of PC-SOM synapses is a long-term feedback mechanism controlling pyramidal cell synaptic plasticity, sufficient to regulate memory consolidation.

KEY WORDS

Optogenetics; inhibitory interneuron; mGluR1a; mTORC1; Schaffer collateral synapse; temporoammonic synapse; pyramidal cell metaplasticity; contextual fear memory

INTRODUCTION

Hippocampal interneurons are heterogeneous populations of GABAergic inhibitory cells with varied morphological, molecular and electrophysiological properties, as well as specialized network functions (Pelkey et al., 2017). CA1 somatostatin-expressing (SOM) cells are a major interneuron subgroup comprised notably of Oriens-Lacunosum/Moleculare (O-LM) cells, bistratified cells and long-range projecting cells (Katona et al., 2014, Pelkey et al., 2017, Honore et al., 2021). SOM cells have axons that target dendrites of pyramidal cells (Muller and Remy, 2014, Lovett-Barron et al., 2014, Klausberger et al., 2003, Pelkey et al., 2017) as well as other interneurons (Fuhrmann et al., 2015, Leao et al., 2012). SOM cells suppress spike rate and burst firing of pyramidal cells in vitro (Lovett-Barron et al., 2012) and of place cells during exploration in vivo (Royer et al., 2012). SOM cells fire with specific phase-coupling during hippocampal theta and gamma network oscillations that are hallmarks of hippocampal function and occur during

spatial navigation, memory tasks, and rapid-eye-movement sleep (Klausberger and Somogyi, 2008, Katona et al., 2014). Indeed, SOM cell regulation of pyramidal neuron activity is critical for hippocampus-dependent learning and memory, as silencing SOM cells during contextual fear conditioning impairs long-term contextual memory (Lovett-Barron et al., 2014).

SOM cells, like other hippocampal interneurons, show long-term synaptic plasticity of their input synapses (Kullmann et al., 2012, Pelletier and Lacaille, 2008, Honore et al., 2021). CA1 pyramidal cell excitatory synapses onto SOM cells (PC-SOM synapses) display a Hebbian form of long-term potentiation (LTP) (Vasuta et al., 2015, Perez et al., 2001, Lapointe et al., 2004, Honore et al., 2021, Croce et al., 2010) dependent on metabotropic glutamate receptor subtype 1a (mGluR1a) activation and postsynaptic Ca^{2+} rise (Lapointe et al., 2004, Perez et al., 2001). This form of long-term plasticity is cell-specific and absent in parvalbumin-expressing cells (Vasuta et al., 2015) and radiatum interneurons (Perez et al., 2001). LTP at input synapses enables long-term regulation of interneuron firing (Croce et al., 2010) and pyramidal cell inhibition (Lapointe et al., 2004).

A critical SOM cell function is the differential regulation of afferents onto pyramidal cell dendrites: via distal dendritic inhibition, SOM cells downregulate activity and LTP in the temporo-ammonic pathway (TA-PC); whereas via proximal dendritic disinhibition (inhibition of other inhibitory interneurons), they upregulate activity and LTP in the CA3-CA1 Schaffer collateral pathway (SC-PC) (Leao et al., 2012). Remarkably, Hebbian LTP at PC-SOM synapses increases subsequent LTP at SC-PC synapses (Vasuta et al., 2015) and decreases subsequent LTP at TA-PC synapses (Sharma et al., 2020), showing that plasticity at PC-SOM input synapses controls durably CA1 network metaplasticity (Honore et al., 2021).

LTP at PC-SOM synapses can be persistent, as repeated activation of mGluR1a induces LTP of excitatory synapses lasting hours and involving gene transcription and mRNA translation (Ran et al., 2009, Artinian et al., 2019). mTORC1 signaling controls translation during LTP at PC-SOM synapses (Ran et al., 2009, Artinian et al., 2019). Interestingly, mTORC1 activity in SOM cells is required for learning-induced LTP of PC-SOM synapses, regulation of CA1 network plasticity, and long-term consolidation of spatial and contextual fear memory (Artinian et al., 2019). However, whether LTP at PC-SOM synapses is sufficient for the regulation of CA1 network metaplasticity and hippocampus-dependent memory remains to be determined.

In the present study, we address this question by using optogenetics to induce long-term plasticity at PC-SOM excitatory synapses. We found that optogenetic stimulation of pyramidal cells induces LTP at PC-SOM synapses in slices. Furthermore, optogenetic induction of LTP at PC-SOM synapses bi-directionally controls CA1 network plasticity by facilitating SC-PC LTP and suppressing TA-PC LTP. Moreover, we uncover that optogenetic induction of LTP at PC-SOM synapses *in vivo* regulates learning-induced LTP at these synapses and controls contextual fear memory. Our findings suggest that LTP at PC-SOM synapses is sufficient to control the state of plasticity in the CA1 network and the consolidation of contextual fear memory, uncovering a long-term feedback control mechanism via PC-SOM synapses sufficient for regulation of CA1 pyramidal cell metaplasticity and hippocampus-dependent memory.

RESULTS

Optogenetically-induced LTP at PC-SOM synapses

CA1 pyramidal cells are the major excitatory synaptic inputs to SOM interneurons in CA1 stratum oriens (Croce et al., 2010, Honore et al., 2021). We used a combination of optogenetic stimulation

after injection of AAV2/9-CaMKIIa-hChR2(E123T/T159C)-mCherry in SOM-Cre-EYFP mice to activate CA1 pyramidal cells, and of whole cell current clamp recordings in slices to monitor excitatory postsynaptic potentials (EPSPs) in CA1 SOM interneurons resulting from activation of PC-SOM synapses (Figure 1A). Local optogenetic stimulation (470 nm) through the objective was adjusted (pulse duration 0.5-2.0 ms) to elicit light-evoked EPSPs in SOM interneurons (Figures 1B-G and S1A-G), similar to EPSPs evoked by electrical stimulation (Figure S2B-F) (Vasuta et al., 2015). Theta burst stimulation (TBS) is an effective induction protocol for eliciting Hebbian LTP at PC-SOM excitatory synapses (Perez et al., 2001, Croce et al., 2010, Vasuta et al., 2015). Therefore, we developed an optogenetic TBS protocol (TBS_{opto}; bursts of 4 light pulses at 80 Hz, given 5 times with 300 ms inter-burst intervals, repeated 3 times at 30 s intervals) effective in eliciting EPSP summation and burst firing of SOM cells (Figure 1B). The TBS_{opto} protocol induced LTP of light-evoked EPSPs at PC-SOM synapses. Light-evoked EPSP amplitude showed a slow onset, gradual increase, lasting at least 30 min after TBS_{opto} (132.0% of baseline at 20-30 min post-induction; Figure 1B and 1J).

Next, we examined the mechanisms involved in the optogenetically-induced LTP at PC-SOM synapses. First, low frequency optogenetic stimulation (LFS_{opto}; 20 Hz) that elicited EPSP summation but a lower rate of firing in SOM cells (Figure 1C) did not induce lasting changes in light-evoked EPSP amplitude (103.0% of baseline at 20-30 min post-induction; Figure 1C and 1J, Figure S1B). Second, in recordings with no optogenetic tetanization, light-evoked EPSP amplitude was unchanged over the same time period (95.7% of baseline at 20-30 min post-induction; Figure 1D and 1J, Figure S1C). Third, to determine whether the optogenetically-induced LTP at PC-SOM synapses was mGluR1a-dependent, TBS_{opto} was given in the presence of the mGluR1a antagonist LY367385 (40 µM) (Figure 1E). In these conditions, TBS_{opto} failed to induce lasting changes in

EPSP amplitude (111.0% of baseline at 20-30 min post-induction; Figure 1E and 1J, Figure S1D). Fourth, to determine whether optogenetically-induced LTP at PC-SOM synapses is dependent on mTORC1-mediated translation, we used SOM-Raptor-KO mice that are deficient in mTORC1 signaling and late-LTP in SOM cells (Artinian et al., 2019). In these mice, TBS_{opto} failed to induce lasting changes in light-evoked EPSP amplitude (104.0% of baseline at 20-30 min post-induction; Figure 1F and 1J, Figure S1E). Fifth, we examined if optogenetically-induced LTP requires transcription by pre-incubating hippocampal slices with 2 μM of the irreversible transcription inhibitor actinomycin D for 15 min prior to recording (Yuan and Burrell, 2013, Younts et al., 2016). In these conditions, TBS_{opto} induced a slow onset LTP of light-evoked EPSP amplitude (119.5% of baseline at 20-30 min post-induction; Figure 1G and 1J, Figure S1F) that was comparable to the LTP induced in control (Figure 1B and 1J) or in vehicle (DMSO; Figure S1G-H). Sixth, we determined if optogenetic stimulation elicited LTP at PC synapses onto parvalbumin-expressing interneurons (PC-Pvalb synapses) using injection of AAV2/9-CaMKIIa-hChR2(E123T/T159C)-mCherry and AAV2/9-EF1a-DIO-EYFP in Pvalb-Cre mice (Figure 1H). In these mice, TBS_{opto} failed to induce lasting increases in light-evoked EPSPs at PC-Pvalb synapses (90.0% of baseline at 20-30 min post-induction; Figure 1I-J, Figure S1I). Together, these results suggest that optogenetic stimulation of CA1 pyramidal cells produces a frequency-dependent LTP at PC-SOM synapses that is dependent on mGluR1a activation and mTORC1-mediated translation, but independent of transcription. Moreover, optogenetic stimulation of CA1 pyramidal cells does not induce LTP at PC-Pvalb synapses.

These properties of optogenetically-induced LTP at PC-SOM synapses are similar to those previously reported for Hebbian LTP at excitatory synapses onto SOM cells characterized using electrical stimulation (Perez et al., 2001, Croce et al., 2010, Honore et al., 2021). So, next we

determined if TBS_{opto} can induce LTP of EPSPs evoked in SOM cells by electrical stimulation (Figure S2A). TBS_{opto} induced a slow onset, gradual LTP, lasting at least 30 min, of electrically-evoked EPSP amplitude (136.0% of baseline at 20-30 min post-induction; Figure S2B and S2G). In control recordings with no optogenetic tetanization, electrically-evoked EPSP amplitude was unchanged over the same time period (103.0% of baseline at 30 min post-induction; Figure S2C and S2G). Also, TBS_{opto} did not induce any change in electrically-evoked EPSP amplitude in SOM cells from mice that received only the control CaMKIIa-mCherry injection without hChR2 (99.7% of baseline at 30 min post-induction; Figure S2D and S2G). TBS_{opto}-induced LTP of electrically-evoked EPSP was mGluR1a-dependent. TBS_{opto} given in the presence of the mGluR1a antagonist LY367385 (40 µM) failed to induce lasting changes in EPSP amplitude (107.0% of baseline at 20-30 min post-induction; Figure S2E and S2G). TBS_{opto}-induced LTP of electrically-evoked EPSPs was also dependent on mTORC1-mediated translation. TBS_{opto} failed to induce lasting changes in electrically-evoked EPSP amplitude in SOM cells of SOM-Raptor-KO mice (97.0% of baseline at 20-30 min post-induction; Figure S2F and S2G). These results indicate that optogenetic theta burst stimulation of CA1 pyramidal cells induces LTP of EPSPs evoked by electrical stimulation via similar mGluR1a- and mTORC1-dependent mechanisms, as at PC-SOM synapses activated optogenetically.

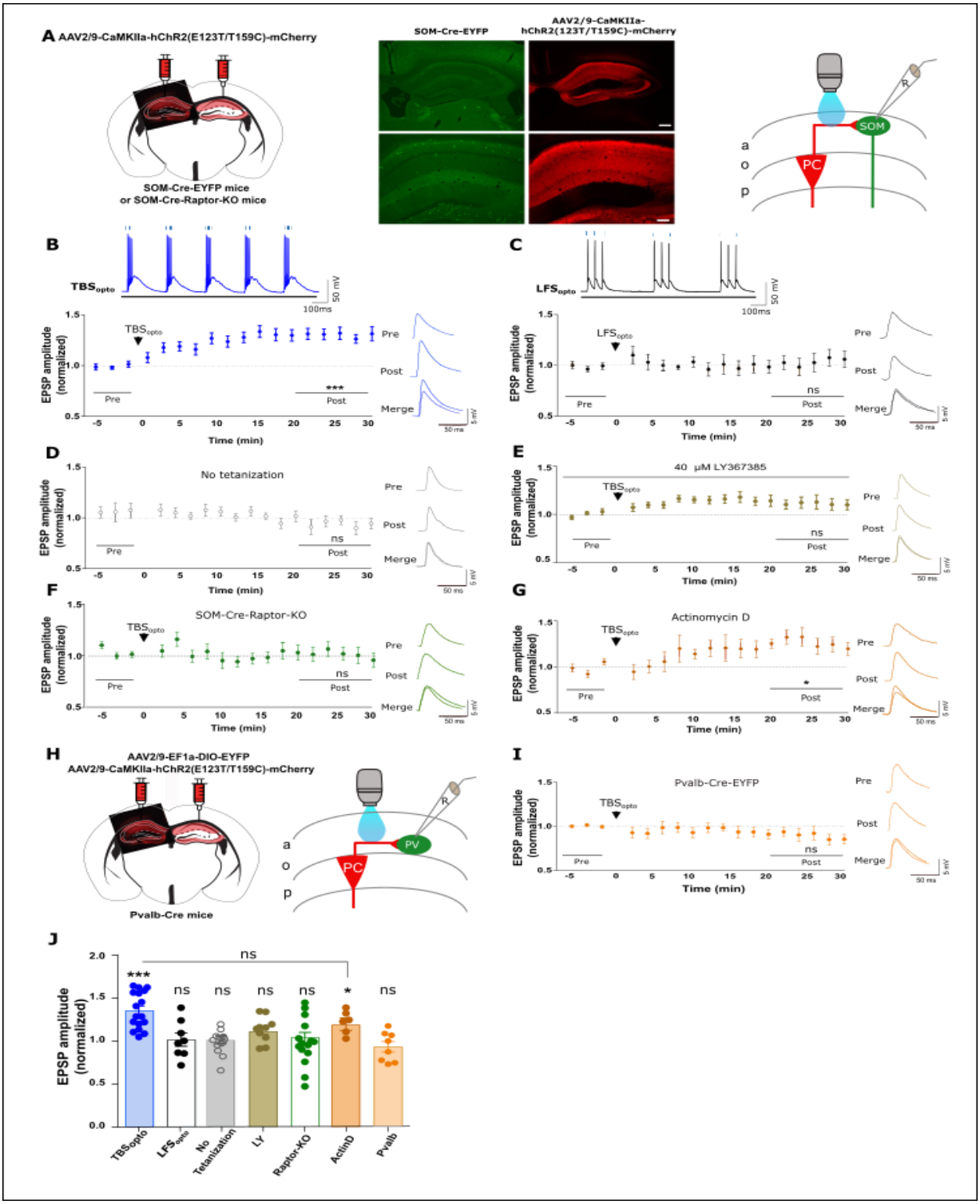
A AAV2/9-CaMKIIa-hChR2(E123T/T159C)-mCherry
SOM-Cre-EYFP mice
or SOM-Cre-Raptor-KO mice
SOM-Cre-EYFP
AAV2/9-CaMKIIa-hChR2(123T/T159C)-mCherry
SOM
PC
a
o
p
B
TBSopto
50 mV
100ms
EPSP amplitude (normalized)
Time (min)
Pre
Post
Merge
***
C
LFSopto
ns
D
No tetanization
E
40 μM LY367385
F
SOM-Cre-Raptor-KO
G
Actinomycin D
*
H
AAV2/9-EF1a-DIO-EYFP
AAV2/9-CaMKIIa-hChR2(E123T/T159C)-mCherry
Pvalb-Cre mice
PV
I
Pvalb-Cre-EYFP
J
TBSopto
LFSopto
No Tetanization
LY
Raptor-KO
ActinD
Pvalb

Figure 1. Optogenetically-induced LTP at PC-SOM synapses. (A) Left: schematic of experimental paradigm showing viral injections in dorsal hippocampus of SOM-Cre-EYFP or SOM-Cre-Raptor-KO mice. Middle: representative images of EYFP expression in SOM cells and mCherry expression in CA1 pyramidal cells (calibration bar: 100 µm bottom; 250 µm top). Right: diagram of local optogenetic stimulation of CA1 pyramidal cells and whole cell recording from SOM interneurons in stratum oriens. (B and C) Bottom left: time plots of light-evoked EPSP amplitude for all SOM cells, showing LTP at PC-SOM synapses following TBS_{opto} (B; n = 17 cells) but not after LFS_{opto} (C; n = 8 cells). Right: example of representative cells of average EPSPs before (Pre) and 20-30 min after (Post) TBS_{opto} or LFS_{opto}. Top: EPSP summation and cell firing during TBS_{opto} (80 Hz) or LFS_{opto} (20 Hz). Paired t-tests; *** $p < 0.0001$; ns, $p > 0.05$. See Figure S1A and S1B for the respective time plots of EPSP amplitude of representative cells in (B) and (C), respectively. (D - G) Left: time plots of light-evoked EPSP amplitude for all SOM cells, showing absence of LTP at PC-SOM synapses following no tetanization (D; n = 13 cells), TBS_{opto} in the presence of the mGluR1a antagonist LY367385 (40 µM) (E; n = 10 cells), or TBS_{opto} in SOM-Cre-Raptor-KO mice (F; n = 15 cells); but LTP after TBS_{opto} in slices pre-incubated with the transcription inhibitor actinomycin D (2µM) (G; n = 6 cells). Right: representative example of average EPSPs before (Pre) and after (Post) each treatment condition. Paired t-tests; * $p < 0.05$; ns, $p > 0.05$. See Figure S1C, S1D and S1F for the respective time plots of EPSP amplitude of representative cells in (D), (E), (F) and (G), respectively; and Figure S1G for representative cell and S1H for time plot for all cells, showing LTP after TBS_{opto} in DMSO (vehicle for actinomycin D). (H) Schematic of experimental paradigm with (left) viral injections in dorsal hippocampus of Pvalb-Cre mice and (right) local optogenetic stimulation of pyramidal cells and recording from CA1 PV interneurons. (I) Time plot of light-evoked EPSP amplitude for all PV cells (left) and example of average EPSPs from a representative cell (right), showing absence of LTP at PC-PV synapses following TBS_{opto} (n = 8 cells). Paired t-test; ns, $p > 0.05$. See Figure S1I for the time plot of EPSP amplitude of the representative PV cell in (I). (J) Summary graph of EPSP amplitude for all cells at 20-30 min post induction, showing LTP after TBS_{opto} in ACSF and after incubation with actinomycin D, but no LTP after LFS_{opto}, in absence of tetanization, or after TBS_{opto} in LY367385, in Som-Cre-RAPTOR mice, or in PV cells. Paired t-tests (Post vs Pre in B-I) and unpaired t-test (Post in B vs Post in G); *** $p < 0.0001$; * $p < 0.05$; ns, $p > 0.05$. Data are represented as mean± SEM here and below. *$p < 0.05$, **$p < 0.01$, ***$p < 0.001$; $p > 0.5$ is considered not significant (ns). Statistical tests and actual p values for each comparison here and below are given in Table S1.

Figure S1. Optogenetically-induced LTP at PC-SOM synapses in representative cells.

Figure S2. Optogenetically-induced LTP of electrically-evoked EPSPs in SOM cells.

TBS_{opto} differentially regulates LTP at Schaffer collateral and temporo-ammonic synapses

CA1 SOM cells (notably OLM cells) differentially control transmission at Schaffer collateral and temporo-ammonic synapses of CA1 pyramidal cells (Leao et al., 2012). In consequence, Hebbian LTP at excitatory synapses onto SOM cells regulates metaplasticity at Schaffer collateral and temporo-ammonic synapses of CA1 pyramidal cells (Vasuta et al., 2015, Artinian et al., 2019, Sharma et al., 2020). So, next we studied if TBS_{opto}-induced LTP at PC-SOM synapses was sufficient to regulate metaplasticity of the CA1 network using whole-field optogenetic stimulation and field potential recordings in slices. First, we established that whole-field optogenetic stimulation also elicited LTP at PC-SOM synapses (Figure 2A). Whole-field TBS_{opto} elicited EPSP summation and burst firing of SOM cells, and induced LTP of light-evoked EPSP amplitude (125.0% of baseline at 20-30 min post-induction; Figure 2B and S3E). LTP was absent in cells that received no optogenetic tetanization (light-evoked EPSP amplitude 97.8% of baseline at 30 min post-induction; Figure S3B and S3E), or with TBS_{opto} given in the presence of the mGluR1a antagonist LY367385 (40 µM) (light-evoked EPSP amplitude 97.0% of baseline at 20-30 min post-induction; Figure S3C and S3E), or in SOM cells of SOM-Raptor-KO mice (light-evoked EPSP amplitude 96.3% of baseline at 20-30 min post-induction; Figure S3D and S3E). Thus, whole-field TBS_{opto} induced a similar mGluR1a- and mTORC1-mediated LTP at PC-SOM synapses as local optogenetic stimulation.

Next, we examined the long-lasting effects of whole-field TBS_{opto} on plasticity at Schaffer collateral synapses (SC-PC synapses) and temporo-ammonic synapses (TA-PC synapses) onto CA1 PCs in slices. First, we investigated regulation of plasticity at SC-PC synapses (Figure 2C and Figure S3F). A weak electrical TBS (wTBS) of the SC pathway failed to induce LTP of fEPSP slope (107.0% of baseline at 25-35 min post-induction; Figure 2D and Figure S3G). In contrast,

when the wTBS was preceded 15 min earlier by TBS_{opto}, LTP was induced at SC-PC synapses (125.7% of baseline at 25-35 min post-induction; Figure 2D and 2F, and Figure S3H). Thus, TBS_{opto} facilitated LTP at SC-PC synapses. In mice with control CaMKIIa-mCherry injection without hChR2, TBS_{opto} failed to facilitate LTP at SC-PC synapses (104.0% of baseline at 25-35 min post-induction; Figure 2D and 2F), indicating that the LTP facilitation was not due to unspecific effects of light stimulation. To determine if the facilitation of LTP at SC-PC synapses was due to plasticity at SOM-PC synapses induced by TBS_{opto}, we examined if the facilitation was dependent on mGluR1a and on mTORC1 in SOM cells. When wTBS was preceded 15 min earlier by TBS_{opto} in the presence of the mGluR1a antagonist LY367385 (40 µM), the facilitation of LTP at SC-PC synapses was absent (107.0% of baseline at 25-35 min post-induction; Figure 2D and 2F). Similarly, when wTBS was preceded 15 min earlier by TBS_{opto} in slices from SOM-Raptor-KO mice, the facilitation of LTP at SC-PC synapses was also absent (112.0% of baseline at 25-35 min post-induction without TBS_{opto} and 1007.0% of baseline at 25-35 min post-induction with TBS_{opto}; Figure 2E and 2F). These results suggests that the facilitation of LTP at SC-PC synapses was due to mGluR1a- and mTORC1-dependent plasticity at SOM-PC synapses induced by TBS_{opto}.

Second, we investigated regulation of plasticity at TA-PC synapses (Figure 2G and Figure S3I). A weak electrical TBS (wTBS) of the TA pathway induced LTP of fEPSP slope (126.7% of baseline at 25-35 min post-induction; Figure 2H and 2J and Figure S3J). In contrast, when the wTBS was preceded 15 min earlier by TBS_{opto}, LTP was prevented at TA-PC synapses (95.5% of baseline at 25-35 min post-induction; Figure 2H and 2J, and Figure S3K). Thus, TBS_{opto} depressed LTP at TA-PC synapses. In mice with control CaMKIIa-mCherry injection without hChR2, TBS_{opto} failed to depress LTP at TA-PC synapses (127.0% of baseline at 25-35 min post-induction;

Figure 2H and 2J), indicating that the LTP depression was not due to unspecific effects of light stimulation. The depression of LTP at TA-PC synapses was likely due to plasticity at SOM-PC synapses induced by TBS_{opto} since it was dependent on mGluR1a and on mTORC1 in SOM cells. The depression of LTP at TA-PC synapses was absent when wTBS was preceded by TBS_{opto} in the presence of the mGluR1a antagonist LY367385 (126.0% of baseline at 25-35 min post-induction; Figure 2H and 2J). Similarly, the depression of LTP at TA-PC was absent when wTBS was preceded by TBS_{opto} in slices from SOM-Raptor-KO mice (123.0% of baseline at 25-35 min post-induction without TBS_{opto} and 118.9% of baseline at 25-35 min post-induction with TBS_{opto}; Figure 2I and 2J). These results suggest that the TBS_{opto}-induced depression of LTP at TA-PC synapses is the result of mGluR1a- and mTORC1-dependent plasticity at SOM-PC synapses. Thus, TBS_{opto}-induced LTP at PC-SOM synapses appears sufficient to regulate metaplasticity of the CA1 network, upregulating LTP at SC-PC synapses and downregulating LTP at TA-PC synapses.

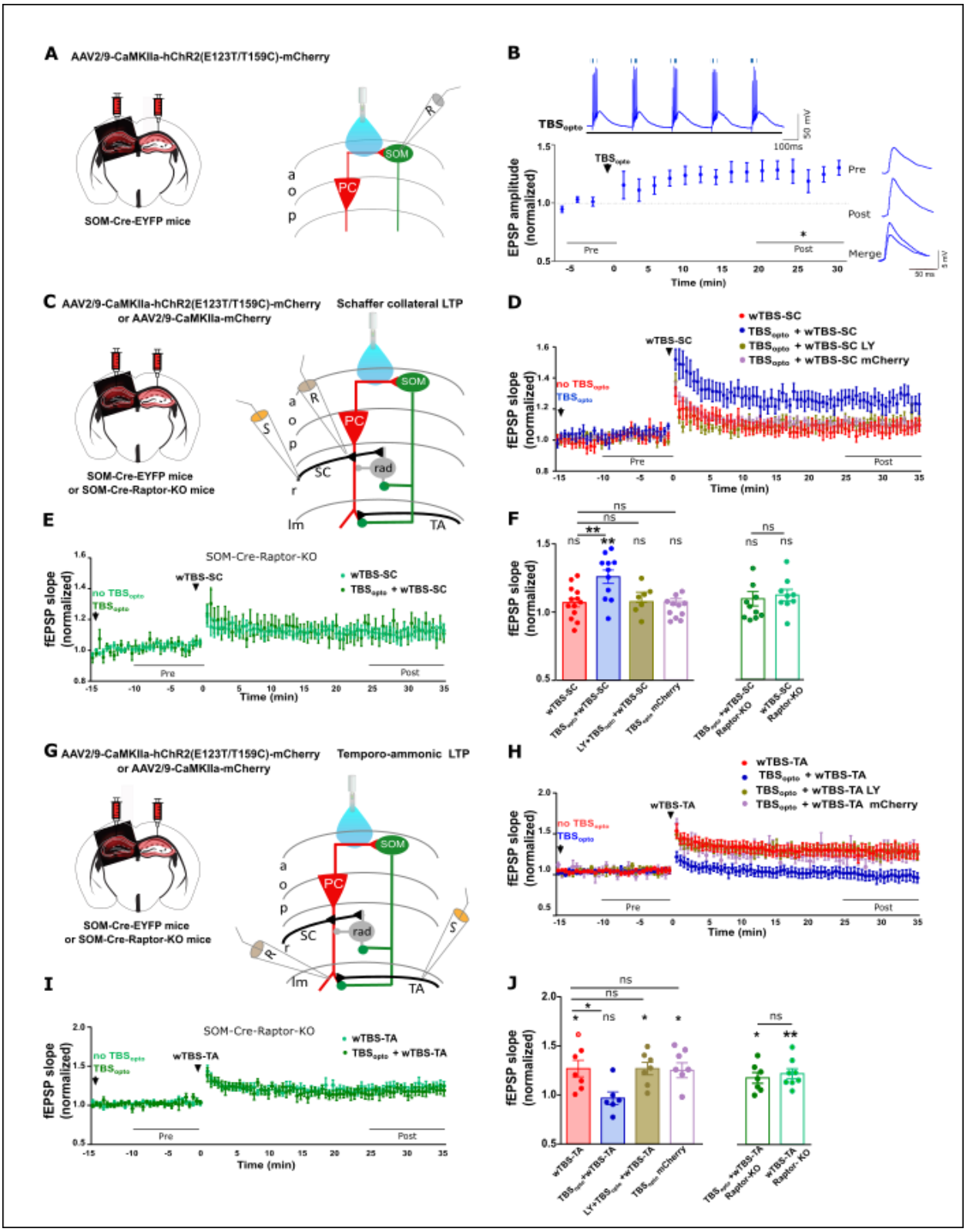
A AAV2/9-CaMKIIa-hChR2(E123T/T159C)-mCherry
SOM-Cre-EYFP mice
SOM
PC
R
a
o
p
B
TBSopto
50 mV
100ms
EPSP amplitude (normalized)
Pre
Post
Merge
Time (min)
C AAV2/9-CaMKIIa-hChR2(E123T/T159C)-mCherry or AAV2/9-CaMKIIa-mCherry
Schaffer collateral LTP
SOM-Cre-EYFP mice or SOM-Cre-Raptor-KO mice
S
SC
rad
lm
TA
D
wTBS-SC
TBSopto + wTBS-SC
TBSopto + wTBS-SC LY
TBSopto + wTBS-SC mCherry
no TBSopto
fEPSP slope (normalized)
Time (min)
E
SOM-Cre-Raptor-KO
wTBS-SC
TBSopto + wTBS-SC
F
ns
**
G AAV2/9-CaMKIIa-hChR2(E123T/T159C)-mCherry or AAV2/9-CaMKIIa-mCherry
Temporo-ammonic LTP
wTBS-TA
TBSopto + wTBS-TA
TBSopto + wTBS-TA LY
TBSopto + wTBS-TA mCherry
H
I
J
*

275

276

Figure 2. Whole-field TBS_{opto} induces LTP at PC-SOM synapses and differentially regulates LTP at SC-PC and TA-PC synapses. (A) Left: schematic of experimental paradigm with hippocampal viral injections in SOM-Cre-EYFP mice. Right: diagram of whole-field optogenetic stimulation of CA1 pyramidal cells and whole cell recording from SOM interneurons. (B) Left bottom: time plot of light-evoked EPSP amplitude for all SOM cells, showing LTP at PC-SOM synapses following TBS_{opto} (n = 7 cells). Left top: EPSP summation and cell firing during TBS_{opto} in a representative cell. Right: example from a representative cell of average light-evoked EPSPs before (Pre) and 20-30 min after (Post) TBS_{opto}. Paired t-test; * $p < 0.05$. See Figure S3A to S3E for the dependence of whole-field TBS_{opto}-induced LTP on tetanization (S3B and S3E), mGluR1a (S3C and S3E) and mTORC1 (S3D and S3E). (C) Left: schematic of experimental paradigm with hippocampal viral injections in SOM-Cre-EYFP or SOM-Cre-Raptor-KO mice. Right: diagram of whole-field optogenetic stimulation of CA1 pyramidal cells, with electrical stimulation and recording of SC-PC fEPSPs in stratum radiatum. (D) Time plot of fEPSP slope for all slices, showing that LTP at SC-PC synapses (n = 13 slices, red) is facilitated by prior application of TBS_{opto} (n = 11 slices, blue), but not in the presence of the mGluR1a antagonist LY367385 (n = 7 slices, brown) nor in slices from mice with control CaMKIIa-mCherry injection without hChR2 (n = 11 slices, magenta). See Figure S3G and S3H for time plots of fEPSP slope in representative slices without and with TBS_{opto}, respectively. (E) Time plot of fEPSP slope for all slices from SOM-Cre-Raptor-KO mice, showing that prior application of TBS_{opto} (n = 10 slices, dark green) does not facilitate LTP at SC-PC synapses (n = 9 slices; light green) in these mutant mice. (F) Summary graph of fEPSP slope for all slices at 25-35 min post induction of LTP at SC-PC synapses, showing that LTP at SC-PC synapses (red) is facilitated by prior application of TBS_{opto} (blue), but not in LY367385 (brown), in slices from mice injected with mCherry (magenta), or in SOM-Cre-Raptor-KO mice (green). Paired t-tests (Pre vs Post); ANOVA, Tukey's multiple comparisons tests (Post wTBS-SC vs Post other conditions); unpaired t-test (wTBS-SC Raptor-KO vs $TBSo_{pto}$ +wTBS-SC Raptor-KO); * $p < 0.05$, ns $p > 0.05$. (G) Left: schematic of experimental paradigm with hippocampal viral injections in SOM-Cre-EYFP or SOM-Cre-Raptor-KO mice. Right: diagram of whole-field optogenetic stimulation of CA1 pyramidal cells, with electrical stimulation and recording of TA-PC fEPSPs in stratum lacunosum-moleculare. (H) Time plot of fEPSP slope for all slices, showing that LTP at TA-PC synapses (n = 7 slices, red) is depressed by prior application of TBS_{opto} (n = 6 slices, blue), but not by TBS_{opto} in the presence of the mGluR1a antagonist LY367385 (n = 7 slices, brown), nor by TBS_{opto} in slices from mice with CaMKIIa-mCherry injection (n = 7 slices, magenta). See Figure S3J and S3K for time plots of fEPSP slope in representative slices without and with TBS_{opto}, respectively.
(I) Time plot of fEPSP slope for all slices from SOM-Cre-Raptor-KO mice, showing that LTP at TA-PC synapses (n = 8 slices; light green) is not depressed by prior application of TBS_{opto} (n = 7 slices, dark green) in these mutant mice. (J) Summary graph of fEPSP slope for all slices at 25-35 min post induction of LTP at TA-PC synapses, showing LTP at TA-PC synapses (red) is depressed by prior application of TBS_{opto} (blue), but not by TBS_{opto} in LY367385 (brown), in slices from mice injected with mCherry (magenta), or in SOM-Cre-Raptor-KO mice (green). Paired t-tests (Pre vs Post); ANOVA, Tukey's multiple comparisons tests (Post wTBS-SC vs Post other conditions); unpaired t-test (wTBS-TA Raptor-KO vs TBS_{opto} +wTBS-TA Raptor-KO); ** $p < 0.01$, * $p < 0.05$, ns $p > 0.05$.
Figure S3. Whole-field TBS_{opto}-induced LTP at PC-SOM synapses and differential regulation of LTP at SC-PC and TA-PC synapses.

TBS_{opto} interferes with contextual fear memory consolidation

At the behavioral level, mTORC1 activity in SOM cells, that is required for learning-induced LTP of PC-SOM synapses, contributes to long-term consolidation of spatial and contextual fear memory (Artinian et al., 2019). So, next we examined if LTP at PC-SOM synapses is sufficient to regulate hippocampus-dependent memory. First, we verified that, as previously reported (Lovett-Barron et al., 2014), activity of CA1 SOM cells is necessary for long-term contextual fear memory using optogenetic silencing of CA1 SOM cells with archaerhodopsin (Arch) (Vasuta et al., 2015) during contextual fear conditioning (Figure 3A and 3B). Optogenetic activation of Arch in phase with the presentation of shocks during conditioning, resulted in reduced freezing during the long-term contextual fear memory test, relative to light stimulation in absence of Arch (51.4% reduction; Figure 3C) or to activation of Arch out of phase (shifted) with presentation of shocks (64.9% reduction; Figure 3C). In the open-field test (Figure S4A), silencing of CA1 SOM cells with light stimulation of Arch did not affect anxiety level (time spent in periphery or center, and ratio of time in center/periphery; Figure S4B) or locomotion (total distance traveled and zone transitions; Figure S4C) relative to mice receiving light stimulation without Arch. These results indicate that silencing SOM cells during contextual fear conditioning impairs long-term contextual fear memory, confirming that SOM cell activity is necessary during long-term contextual fear learning (Lovett-Barron et al., 2014).

Next, we determined if LTP at PC-SOM synapses is sufficient to regulate hippocampus-dependent memory by using the TBS_{opto} induction protocol that elicit LTP at PC-SOM synapses in slices and investigating its effect in vivo on contextual fear memory after CA1 injection of AAV2/9-CaMKIIa-hChR2(E123T/T159C)-mCherry in SOM-Cre-EYFP mice (Figure 3D and 3E). TBS_{opto} given in CA1 30 min prior to conditioning resulted in reduced freezing during the

long-term contextual fear memory test, relative to mice receiving no TBS_{opto} prior to conditioning (73.7% reduction; Figure 3F) or TBS_{opto} in the absence of hChR2 (71.5% reduction; Figure 3F). Mice in the three groups showed similar normal anxiety level (time spent in periphery or center, and ratio of time in center/periphery; Figure S4E) and locomotion (total distance traveled and zone transitions; Figure S4F) in the open-field test. These results indicate that the TBS_{opto} induction protocol that elicit LTP at PC-SOM synapses is sufficient to regulate long-term contextual fear memory in vivo.

Since LTP induced by TBS_{opto} at PC-SOM synapses, and its regulation of CA1 PC metaplasticity, are blocked by conditional knock-out of *Rptor* in SOM cells (Figures 1 and 2), we tested next if the reduction of fear memory by TBS_{opto} was due to mTORC1 signaling in SOM cells. TBS_{opto} in CA1 given 30 min prior to conditioning in SOM-Cre-Raptor-KO mice did not affect freezing during the long-term contextual fear memory test, relative to mice not receiving TBS_{opto} prior to conditioning (Figure 3F). Both mice groups behaved similarly in the open-field test (Figure S4D-S4F) indicating normal anxiety level and locomotion. These results indicate that the TBS_{opto}-induced impairment of fear memory was dependent on mTORC1 signaling in SOM interneurons and not due to other non-specific effects of optogenetic activation of CA1 PCs, suggesting that TBS_{opto}-induced LTP at PC-SOM synapses is sufficient for the regulation of hippocampus-dependent memory.

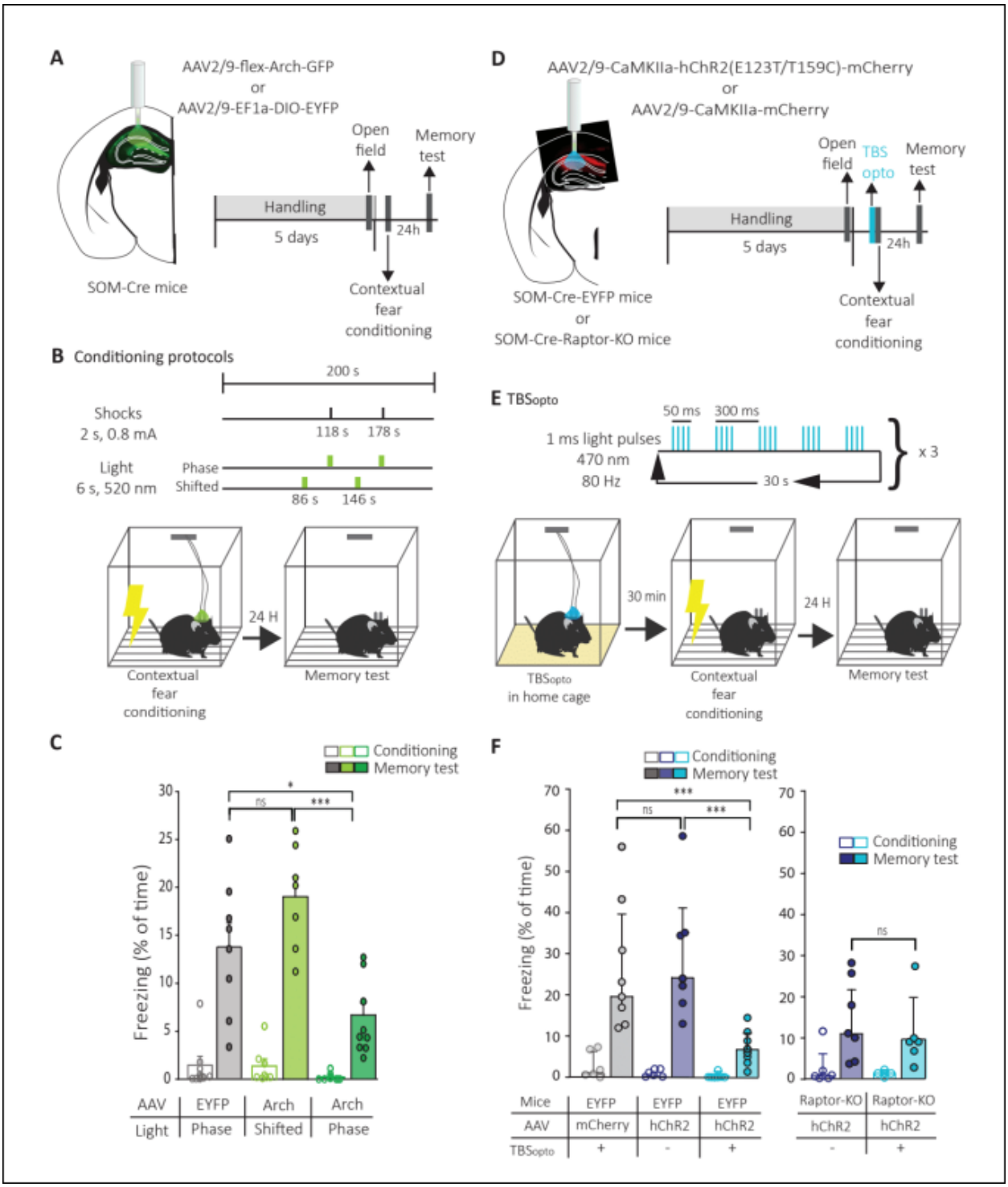
A
AAV2/9-flex-Arch-GFP
or
AAV2/9-EF1a-DIO-EYFP
Open field
Memory test
Handling
5 days
24h
SOM-Cre mice
Contextual fear conditioning
D
AAV2/9-CaMKIIa-hChR2(E123T/T159C)-mCherry
or
AAV2/9-CaMKIIa-mCherry
Open field
TBS opto
Memory test
Handling
5 days
24h
SOM-Cre-EYFP mice
or
SOM-Cre-Raptor-KO mice
Contextual fear conditioning
B Conditioning protocols
200 s
Shocks
2 s, 0.8 mA
118 s
178 s
Light
6 s, 520 nm
Phase
Shifted
86 s
146 s
24 H
Contextual fear conditioning
Memory test
E TBSopto
50 ms
300 ms
1 ms light pulses
470 nm
80 Hz
x 3
30 s
30 min
24 H
TBSopto in home cage
Contextual fear conditioning
Memory test
C
Conditioning
Memory test
Freezing (% of time)
ns
***
*
AAV
Light
EYFP
Phase
Arch
Shifted
Arch
Phase
F
Conditioning
Memory test
Freezing (% of time)
Mice
AAV
TBSopto
EYFP
mCherry
+
EYFP
hChR2
-
EYFP
hChR2
+
Raptor-KO
hChR2
-
Raptor-KO
hChR2
+

Figure 3. Silencing of SOM cells and TBS_{opto} impair contextual fear memory. (A) Left: schematic of cannulation and injection site of AAV2/9-flex-Arch-GFP or AAV2/9-EF1a-DIO-EYFP in dorsal CA1 hippocampus of SOM-Cre mice with representative image of Arch expression. Right: diagram of behavioral testing sequence (open field and contextual fear conditioning). (B) Experimental protocol of optogenetic stimulation (in phase or shifted with respect to shocks) during contextual fear conditioning. (C) Summary graph for all mice, showing reduced freezing in the long-term memory test in mice that received Arch activation in phase with shocks (n=9 mice, dark green), relative to those that received light stimulation without Arch (n=8 mice, gray) or Arch activation out of phase with shocks (shifted; n=7 mice, light green). One way ANOVA, Holm-Sidak pair-wise comparisons, * $p<0.05$, *** $p<0.001$, ns $p>0.05$. (D) Schematic of cannulation and injection site of AAV2/9-CaMKIIa-hChR2(E123T/T159C)-mCherry or AAV2/9-CaMKIIa-mCherry in dorsal CA1 hippocampus of SOM-Cre-EYFP or SOM-Cre-Raptor-KO mice with a representative image of hChR2-mCherry expression, and diagram of behavioral testing sequence (open field and contextual fear conditioning). (E) Experimental protocol of TBS_{opto} given 30 min prior to contextual fear conditioning. (F) Left: Summary graph for all SOM-Cre-EYFP mice, showing reduced freezing in the long-term memory test in mice that received TBS_{opto} (n=8 mice, blue), relative to mice that received no TBS_{opto} (n=7 mice, violet) or TBS_{opto} without hChR2 (n=8 mice, gray). Kruskal-Wallis One-way ANOVA on Ranks, Dunn's pair-wise comparisons test, *** $p=0.001$, ns $p>0.05$. Right: Similar data presentation for SOM-Cre-Raptor-KO mice, showing no difference in freezing in the long-term memory test in mice that received TBS_{opto} (n=6 mice, blue) or no TBS_{opto} (n=7 mice, violet). Unpaired t-test, ns $p>0.05$.

Figure S4 Normal anxiety and locomotion in open-field tests.

Prior induction of LTP by TBS_{opto} results in subsequent TBS- and learning-induced depotentiation

Since the behavior experiments indicate that TBS_{opto} impairs contextual fear memory consolidation when given prior to contextual fear conditioning, we examined the interaction between optogenetically- and electrically-induced LTP of electrically-evoked EPSPs in SOM cells in slices (Figure 4A).

After a baseline period, a first episode of electrical TBS elicited LTP of EPSP amplitude (134.0% of baseline at 10-15 min post-induction TBS#1), and a second TBS episode induced a further increase in LTP (164.0% of baseline at 30-35 min post-induction TBS#1; Figure 4B). In contrast, a first episode of TBS_{opto} elicited LTP of EPSP amplitude (140.0% of baseline at 10-15 min post-induction of TBS_{opto} #1), and a second TBS_{opto} episode did not induce a further increase in LTP (142.0% of baseline at 30-35 min post-induction TBS_{opto} #1; Figure 4C). Interestingly, after a first episode of TBS_{opto} that elicited LTP of EPSP amplitude (121.0% of baseline at 10-15 min post-induction of TBS_{opto} #1), a subsequent TBS episode induced depotentiation of EPSP amplitude (94.0% of baseline at 30-35 min post-induction TBS_{opto} #1; Figure 4D). Such a depotentiation was absent when a first episode of TBS (130.0% of baseline at 10-15 min post-induction of TBS #1) was followed by a subsequent TBS_{opto} episode (141.0% of baseline at 30-35 min post-induction TBS #1; Figure 4E). Finally, a single TBS episode given at the later time point induced LTP (129.0% of baseline; Figure 4F), suggesting that the depotentiation induced by TBS was not due to a response run-down due to recording time, or dialysis of cell content. Thus, prior induction of LTP by TBS_{opto} engages some mechanisms resulting in depotentiation when TBS is given subsequently.

Contextual fear conditioning induces a persistent LTP of PC-SOM synapses, that can be recorded ex vivo 24h after conditioning (Artinian et al., 2019). Therefore, we used ex vivo whole cell recordings in slices 24 hours after conditioning, to examine if in vivo TBS_{opto} given 30 min prior to contextual fear conditioning interferes with learning-induced LTP at excitatory synapses of SOM cells (Figure 4G). SOM cells from mice that received TBS_{opto} prior to contextual fear conditioning exhibited decreases in spontaneous EPSC frequency and amplitude, relative to cells from mice with contextual fear conditioning only (56.1% decrease in frequency, 31.9% decrease in amplitude: Figure 4H). Similarly, the input-output function of electrically-evoked EPSCs was decreased in SOM cells from mice that received TBS_{opto} prior to contextual fear conditioning, relative to cells from mice with contextual fear conditioning only (64.1% decrease in slope of EPSC input-output function; Figure 4I). These results suggest that in vivo TBS_{opto} given 30 min prior to contextual fear conditioning interferes with learning-induced LTP at PC-SOM synapses, consistent with our findings thatinduction of Hebbian LTP results in depotentiation at PC-SOM synapses after prior induction of LTP by TBS_{opto} in slices. Overall, our findings indicate that LTP at PC-SOM synapses is sufficient to regulate CA1 pyramidal cell metaplasticity and hippocampus-dependent memory.

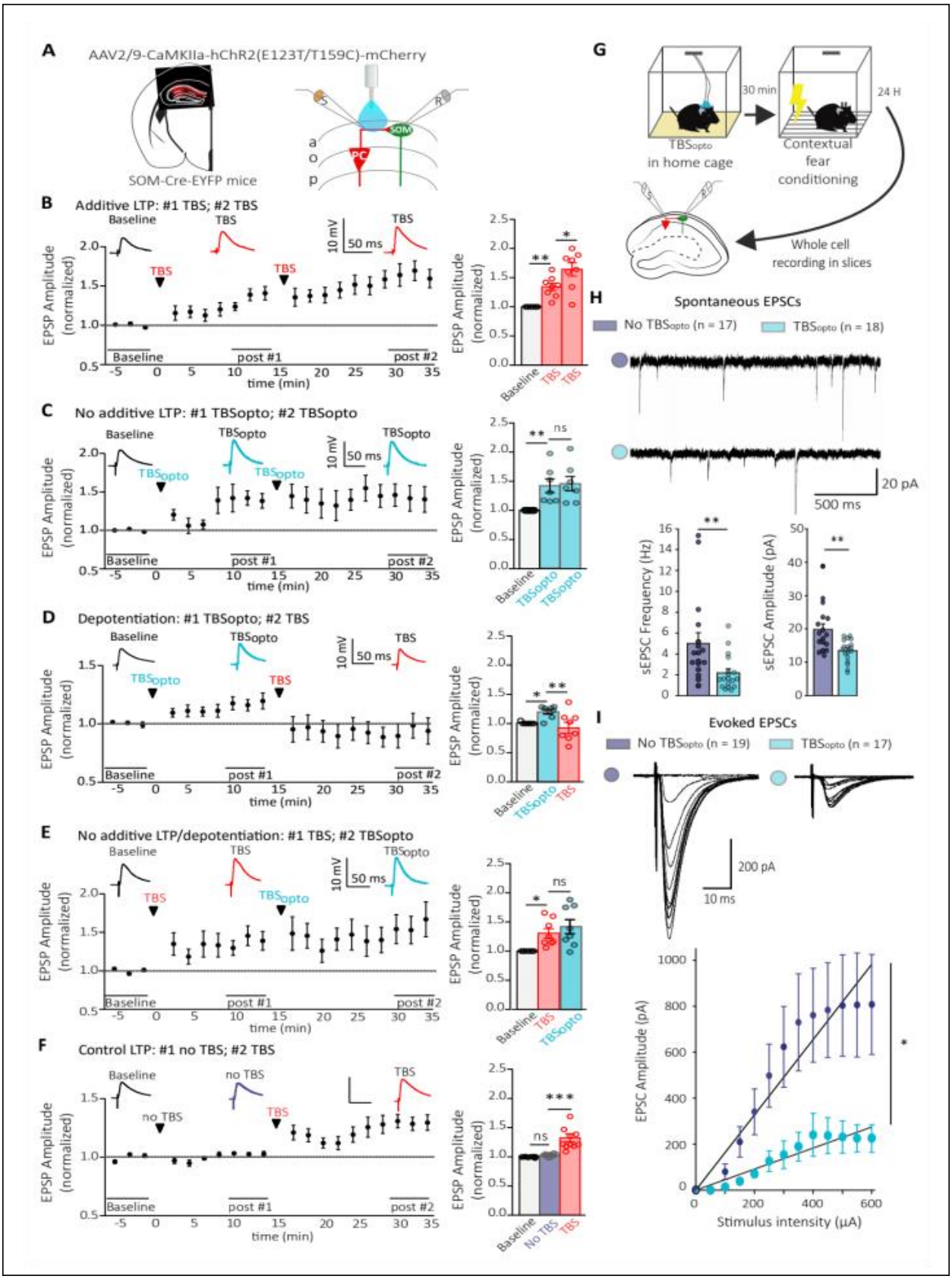
A
AAV2/9-CaMKIIa-hChR2(E123T/T159C)-mCherry
SOM-Cre-EYFP mice
SOM
PC
a
o
p
B
Additive LTP: #1 TBS; #2 TBS
Baseline
TBS
10 mV
50 ms
EPSP Amplitude (normalized)
time (min)
post #1
post #2
C
No additive LTP: #1 TBSopto; #2 TBSopto
TBSopto
ns
D
Depotentiation: #1 TBSopto; #2 TBS
E
No additive LTP/depotentiation: #1 TBS; #2 TBSopto
F
Control LTP: #1 no TBS; #2 TBS
no TBS
G
30 min
24 H
TBSopto in home cage
Contextual fear conditioning
Whole cell recording in slices
H
Spontaneous EPSCs
No TBSopto (n = 17)
TBSopto (n = 18)
20 pA
500 ms
sEPSC Frequency (Hz)
sEPSC Amplitude (pA)
I
Evoked EPSCs
No TBSopto (n = 19)
TBSopto (n = 17)
200 pA
10 ms
EPSC Amplitude (pA)
Stimulus intensity (μA)

452

Figure 4. LTP induction by TBS_{opto} interferes with subsequent induction of Hebbian or learning-related LTP. (A) Left: schematic of experimental paradigm with viral injections in dorsal hippocampus of SOM-Cre-EYFP. Right: diagram of whole-field optogenetic stimulation of CA1 pyramidal cells (TBS_{opto}), electrical stimulation of afferents in stratum oriens/alveus (S), and whole cell recording (R) of electrically-evoked EPSPs in SOM interneurons. (B-F) (Left) Time plots of electrically-evoked EPSP amplitude for all cells (with above, representative average EPSPs during baseline, post induction #1 and #2), and (right) summary bar graphs of EPSP amplitude for all cells during baseline, 10-15 min after induction #1 and 15-20 min after induction #2, showing: (B) LTP following a first episode of TBS of afferents (TBS#1) that is further increased after a second TBS episode (n = 8 cells); (C) LTP following a first episode of TBS_{opto} without further increase following a second TBS_{opto} episode (n = 7 cells); (D) LTP following a first episode of TBS_{opto} followed by depotentiation after a subsequent episode of TBS (n = 8 cells); (E) LTP following a first episode of TBS and absence of depotentiation after a subsequent TBS_{opto} episode (n = 8 cells); and (F) LTP following TBS given at the induction #2 time point only (n = 10 cells). rmANOVA, Tukey's multiple comparisons test; * $p < 0.05$, ** $p < 0.01$, *** $p < 0.0001$, ns $p > 0.05$. (G) Diagram of experimental paradigm with in vivo optogenetic stimulation of CA1 pyramidal cells (TBS_{opto}) prior to contextual fear conditioning, and ex vivo whole cell recording of spontaneous and electrically-evoked EPSCs (electrical stimulation in stratum oriens/alveus) in SOM interneurons in slices at 24 hours post conditioning. (H) Top: Spontaneous EPSCs from representative cells from mice receiving contextual fear conditioning only (violet) or TBS_{opto} prior to contextual fear conditioning (blue). Bottom: Summary bar graphs of sEPSC frequency and amplitude for all cells, showing decrease in frequency and amplitude of sEPSCs in cells from mice with TBS_{opto} prior to contextual fear conditioning (blue; n = 18 cells, 3 mice), relative to cells from mice with contextual fear conditioning only (violet; n = 17 cells, 4 mice). Mann-Whitney Rank Sum Test, ** $p < 0.01$. (I) Top: Family of EPSCs evoked by increasing intensity of stimulation in representative cells from mice receiving contextual fear conditioning only (violet) or TBS_{opto} prior to contextual fear conditioning (blue). Bottom: Summary plots of input-output function of EPSC amplitude as a function of stimulation intensity and linear fit (synaptic gain), showing that the input-output function of evoked EPSCs was decreased in cells from mice with TBS_{opto} prior to contextual fear conditioning (blue; n = 17 cells, 3 mice), relative to cells from mice that received contextual fear conditioning only (violet; n = 19 cells, 4 mice). Mann-Whitney Rank Sum Test, * $p < 0.05$.

DISCUSSION

Long-term synaptic plasticity at excitatory input synapses onto specific inhibitory interneurons is an intriguing feature of hippocampal synaptic networks but its role in hippocampal memory function has remained largely undetermined (Kullmann et al., 2012, Honore et al., 2021, Bartos et al., 2011, McBain and Kauer, 2009). Brain-wide manipulation mTORC1 activity specifically in SOM cells indicated that LTP at afferent synapses of hippocampal SOM cells contributes to regulation of CA1 network plasticity and long-term consolidation of spatial and contextual fear memory (Artinian et al., 2019). Here we used hippocampal CA1-specific optogenetic approaches to establish that LTP at PC-SOM synapses is sufficient to differentially control metaplasticity of SC-PC and TA-PC synapses, and regulate contextual fear memory, uncovering a long-term feedback mechanism controlling pyramidal cell synaptic plasticity and memory consolidation.

TBS_{opto}-induced LTP

TBS_{opto} was sufficient to induce LTP of synaptic responses elicited by optogenetic activation or local electrical stimulation of PC-SOM synapses. Optogenetically-induced LTP at PC-SOM synapses shared key features with Hebbian LTP induced by electrical tetanization: slow onset potentiation, frequency-dependence, mGluR1a-mediated, and SOM *versus* Pvalb cell-specificity (Perez et al., 2001, Lapointe et al., 2004, Croce et al., 2010, Vasuta et al., 2015). Since TBS_{opto} restricts activation to CA1 PCs, without affecting other CA1 afferent fibers potentially activated with tetanization by electrical stimulation (Nabavi et al., 2014, Nicholson and Kullmann, 2021, Cardin et al., 2010), selective activation of CA1 PC axons may, thus, be sufficient to induce Hebbian LTP at PC-SOM synapses. CA1 SOM cells receive other afferents, notably cholinergic projections from septum (Lovett-Barron et al., 2012, Leao et al., 2012), GABAergic fibers from

septum (Sun et al., 2014), brainstem nucleus incertus (Szonyi et al., 2019) and local interneurons (Tyan et al., 2014), as well as noradrenergic, serotonergic and dopaminergic inputs (Pelkey et al., 2017, Oleskevich et al., 1989). Our findings establish that activation of these other projection systems is not required for LTP at PC-SOM synapses. This is in contrast to another form of plasticity at excitatory synapses onto putative-SOM cells in CA1 stratum oriens, anti-Hebbian LTP (Lamsa et al., 2007, Nicholson and Kullmann, 2021), which can be induced by optogenetic activation of cholinergic afferents but not of CA1 PCs, and, thus, is due to cholinergic heterosynaptic LTP at PC-oriens interneurons excitatory synapses (Nicholson and Kullmann, 2021). Our finding that TBS_{opto} of PC-SOM synapses is sufficient for induction of LTP is consistent with previous work that Hebbian LTP is afferent pathway-specific, occurring at CA1 PC-SOM synapses but not at CA3 PC-SOM synapses (Croce et al., 2010).

Interestingly, we uncovered that TBS_{opto}-induced LTP at PC-SOM synapses was mTORC1-dependent and transcription-independent. A more persistent (lasting many hours) form of mGluR1a-mediated LTP at PC-SOM synapses is both transcription- and translation-dependent (Ran et al., 2009, Artinian et al., 2019). Since mTORC1 is a key signaling control mechanism of translation (Costa-Mattioli et al., 2009), our results suggest that mGluR1a-mediated LTP at PC-SOM synapse is translation-dependent. Thus, LTP at PC-SOM synapses may be mediated by mechanisms analogous to mGluR-mediated, mTORC1- and translation-dependent, transcription-independent LTD at SC-PC synapses (Huber et al., 2000, Banko et al., 2006). Such a mTORC1- and protein synthesis-dependent mechanism is consistent with the slow onset gradual development over minutes of LTP at PC-SOM synapses (Huber et al., 2000).

Network regulation

Our finding that TBS_{opto} up-regulated LTP at SC-PC synapses and down-regulated LTP at TA-PC synapses in a mGluR1a- and SOM cell-mTORC1-dependent manner, is consistent with a differential gating of plasticity at PC input pathways by SOM cells (Leao et al., 2012) that is controlled over long-term periods by plasticity of SOM cell input synapses (Vasuta et al., 2015, Artinian et al., 2019, Sharma et al., 2020, Leao et al., 2012). It is noteworthy that TBS_{opto} did not affect basal transmission at SC- and TA-PC synapses, but regulated theta burst induced plasticity at these synapses. This modulation of plasticity reflects the property of PC-SOM synapses that show facilitation and postsynaptic firing with repeated stimulation, resulting in effective recruitment with repetitive activation of PCs (Croce et al., 2010, Honore et al., 2021, Pouille and Scanziani, 2004).

Our findings highlight the different roles of long-term synaptic plasticity at excitatory synapses onto PC *versus* SOM interneurons. It has been proposed that LTP at PC excitatory synapses serves to generate enduring changes at synapses of engram cells that encode memories (Nabavi et al., 2014, Choi et al., 2018). In contrast, our results suggest that LTP at SOM cell excitatory synapses may serve to regulate the state of plasticity (or metaplasticity) of PC input synapses (Honore et al., 2021). These distinct roles suggest that hippocampal-dependent encoding of memories, via LTP in PCs, can still occur, albeit in a reduced manner, in the absence of LTP at SOM cell synapses, as for example in mice with conditional knockout of *Rptor* in SOM cells (Artinian et al., 2019). However, LTP at PC-SOM synapses controls the efficiency of hippocampal-dependent encoding memories by PCs, providing additional versatility to CA1 network plasticity.

The gating of PC input pathways has been well established for OLM cells, a subtype of SOM cells (Leao et al., 2012). However, SOM cells also include other types of interneurons:

bistratified cells, and other cells with both local projections and distal projections to septum, subiculum or retrohippocampal areas (CA3, dentate gyrus, entorhinal cortex) (Honore et al., 2021, Pelkey et al., 2017, Booker and Vida, 2018). Although excitatory synapses onto bistratified cells and OLM cells show Hebbian LTP (Perez et al., 2001, Croce et al., 2010), it remains to be determined if SOM projection cells also do. Thus, it will be interesting to build on our findings and determine how plasticity at input synapses of other CA1 SOM cell types may participate in network regulation, possibly even controlling more distant hippocampal-related pathways.

Learning-induced changes at the input synapses of SOM cells may only be part of a more integrated response of SOM cells during learning. An increase in the intrinsic excitability of CA1 SOM cells, due to a reduced Ca^{2+}-dependent K^{+} conductance, was found after learning a hippocampus-dependent trace eyeblink conditioning task (McKay et al., 2013). Although it remains to be determined if SOM cell inhibitory synapses demonstrate learning-induced changes (Chiu et al., 2018, Udakis et al., 2020), mTORC1-dependent axonal sprouting by CA1 SOM cells takes place in the CACNA1A mouse model of epilepsy which is characterized by impaired synaptic inhibition by Pvalb interneurons (Jiang et al., 2018). These previous works and our findings indicate that multiple plasticity mechanisms occur in SOM cells at the level of their input function, intrinsic excitability and perhaps even output synapses, suggesting that an integrated gain-of-function response may occur in SOM cells during learning.

TBS_{opto} interaction with Hebbian and learning-induced LTP

Our results indicate that LTP at PC-SOM synapses induced by TBS_{opto} share similar mechanisms as Hebbian LTP induced by electrical TBS and LTP induced by contextual fear learning at excitatory synapses onto SOM cells. As reported for LTP at hippocampal synapses (Bliss and

Lomo, 1973), LTP induced by a first episode of TBS_{opto} occluded further LTP by a second TBS_{opto}. However, LTP induced by a first episode of electrical TBS did not, and more LTP was induced by a second episode of TBS. In contrast, when electrical TBS was given after LTP induced by a first TBS_{opto} episode, depotentiation occurred at PC-SOM synapses. Similarly, in vivo, when contextual fear conditioning was given 30 min after TBS_{opto}, the efficacy of PC-SOM synapses was reduced during *ex vivo* recordings 24 hours later. These results indicate that although they share similar mechanisms, LTP induced by TBS_{opto}, electrical TBS and fear learning are not identical. This is not surprising given that electrical stimulation may activate additional intra-hippocampal fibers, and learning may implicate other systems in addition to CA1 PC-SOM synapses. These additional mechanisms are likely implicated in the depotentiation of PC-SOM synapses. Multiple mechanisms regulate PC-SOM synapse function and plasticity, notably pre- and post-synaptic $GABA_B$-receptor mediated inhibition (Booker et al., 2020, Booker et al., 2018), astrocyte-mediated regulation of glutamate uptake (Huang et al., 2004), and $GABA_A$ synaptic inhibition by vasoactive intestinal polypeptide inhibitory interneurons (Tyan et al., 2014). It will be important to determine if any of these control mechanisms are implicated in the modulation/depotentiation of PC-SOM synapses. Importantly, our findings that learning-induced potentiation is impaired by prior application of TBS_{opto} *in vivo* may explain why contextual fear memory may be impaired by TBS_{opto}, providing further support that LTP induced at PC-SOM synapses is sufficient to regulate CA1 network metaplasticity and the contextual fear memory.

MATERIAL AND METHODS

Animals

Experimental protocols were approved by the Animal Care Committee at the Université de Montréal (Comité de Déontologie de l'Expérimentation sur les Animaux; CDEA Protocols # 17-001, 17-002, 18-002, 18-003, 19-003, 19-004, 20-001, 20-002, 21-001, 21-002) and experiments were performed in accordance with the Canadian Council of Animal Care guidelines.

Sst$^{\text{ires-Cre}}$ mice (Taniguchi et al., 2011) were crossed with *Rosa26*$^{\text{lsl-EYFP}}$ reporter mice (Madisen et al., 2010) to generate Cre-dependent Enhanced Yellow Fluorescent Protein (EYFP) expression in SOM interneurons (SOM-Cre-EYFP mice) (Artinian et al., 2019). *Sst*$^{\text{ires-Cre}}$;*Rosa26*$^{\text{lsl-EYFP}}$ mice were crossed with floxed *Rptor* mice (Sengupta et al., 2010) for cell-specific homozygous knock-out of *Rptor* in SOM cells (SOM-Cre-Raptor-KO mice) (Artinian et al., 2019). *Pvalb*$^{\textit{ires}\text{-Cre}}$ mice (Hippenmeyer et al., 2005) were used for Cre-dependent targeting of PV interneurons (Pvalb-Cre mice). Mice were housed 2-4 animals per cage, except for *in vivo* optogenetic studies in which mice were housed singly after cannula implantation. Food and water were *given ad libitum*. The mice were maintained on a 12 h light/dark cycle with all experiments performed during the light phase.

The *in vitro* electrophysiological slice experiments were performed on 6-7 weeks old male or female mice at the diestrus phase to reduce possible variability in responses. Behavioral studies and *ex vivo* electrophysiological slice experiments were carried out on 8-10 weeks old male mice.

Virus injection

Four weeks old mice were given an intraperitoneal (IP) injection of ketamine (50 mg/kg i.p.) and xylazine (5 mg/kg i.p.) and placed in a stereotaxic frame (Stoelting). For *in vitro* slice experiments, AAV2/9-CaMKIIa-hChR2(E123T/T159C)-mCherry ($1.5\text{-}1.77\times10^{12}$ particles/ml) or AAV2/9-CaMKIIa-mCherry (2.20×10^{13} particles/ml) were injected bilaterally in CA1 hippocampus

(coordinates relative to bregma: −1.95 mm AP, ±1.3 mm ML, and -1.3 mm DV) of mice of either sex. Viral solution (0.5-0.8µl) was delivered at a flow rate of 50-100 nl/min using a 10µl Hamilton syringe and a microfluidic pump (Harvard Apparatus). The needle was left in place for at least 5 minutes after injection. For some slice experiments, Pvalb-Cre mice were injected, in addition, with AAV2/9-EF1a-DIO-EYFP (3.95×10^{13} particles/ml). For *in vivo* optogenetic experiments, 7-8 weeks old male mice were used and treated as above. In some *in vivo* experiments, mice were injected bilaterally 0.5µl of AAV2/9-flex-Arch-GFP ($1.74\text{-}1.83\times10^{13}$ particles/ml) or AAV2/9-EF1a-DIO-EYFP (3.95×10^{13} particles/ml) as above.

Hippocampal slice preparation

Six to seven weeks old animals (10-18 days after viral injection) were anesthetized by isoflurane inhalation and the brain was rapidly removed and placed in cold (4°C) sucrose-based cutting solution saturated with 95% O_2 and 5% CO_2 containing the following (in mM): 87 NaCl, 2.5 KCl, 1.25 NaH_2PO_4, 7 $MgSO_4$, 0.5 $CaCl_2$, 25 $NaHCO_3$, 25 glucose, 9.5 ascorbic acid, 3.0 pyruvic acid and 75 sucrose, pH 7.4, and 295-300 mOsmol/L. A block of tissue containing the hippocampus was prepared and transverse hippocampal slices (300 and 400 µm thickness for whole-cell and field recordings, respectively) were cut with a vibratome (Leica VT1000S). Slices were transferred to artificial CSF (ACSF; saturated with 95% O_2 and 5% CO_2) containing the following (in mM): 124 NaCl, 2.5 KCl, 1.25 NaH_2PO_4, 4 $MgSO_4$, 4 $CaCl_2$, 26 $NaHCO_3$, and 10 glucose (pH 7.3–7.4, and 295–300 mOsmol/L) at 32°C for 30 minutes, and afterward maintained at room temperature (20–22°C) for at least 90 minutes and until recording experiments. Individual slices were transferred to a submersion chamber perfused (3-4 ml/min) with ACSF at 31 ± 0.5°C, and with CA1 and CA3 regions separated by a surgical cut. For *ex vivo* recordings after learning, slices were

obtained as above from animals 24 hours after optogenetic stimulation and contextual fear conditioning.

Whole-cell patch clamp recording

EYFP-expressing CA1 interneurons were identified using an upright microscope (Nikon Eclipse, E600FN), equipped with a water-immersion long-working distance objective (40x; differential interference contrast, DIC), epifluorescence and an infrared CCD camera (CXE-B013-U; Mightex). Whole-cell current-clamp recordings were obtained using borosilicate glass pipettes (3-5 MΩ) filled with intracellular solution containing (in mM): 120 $KMeSO_4$, 10 KCl, 0.5 EGTA, 10 HEPES, 2.5 MgATP, 0.3 NaGTP and 10 Na_2-phosphocreatine (pH 7.3, 290-298 mOsmol/L). For whole-cell voltage-clamp recordings, the intracellular solution contained (in mM): 120 $CsMeSO_3$, 5 CsCl, 2 $MgCl_2$, 10 HEPES, 0.5 EGTA, 10 Na_2-phosphocreatine, 2 ATP-Tris, 0.4 GTP-Tris, 0.1 spermine, 2 QX314 (pH 7.2–7.3, 300 mOsmol/L). Data was acquired using a Multiclamp 700B amplifier (Molecular Devices) and digitized at 10-20 kHz using Digidata 1440A and pClamp 10.5/10.7 software (Molecular Devices). Recordings were low-pass filtered at 2 kHz and membrane potential was corrected for liquid junction potential (11 mV). Access resistance was monitored throughout experiments and data were included only if the holding current and series resistance were stable (changes <20% of initial value).

Whole cell recording of synaptic responses

EPSPs and EPSCs evoked by electrical stimulation were elicited using constant current pulses (50 µs duration) via an ACSF-filled bipolar theta-glass electrode positioned approximately 100-150 µm lateral from the recorded cell soma near the border between CA1 stratum oriens and the alveus.

EPSCs were recorded in the presence of DL-2-Amino-5-phosphonopentanoic acid (DL-AP5; 50 µM) and SR-95531 (Gabazine, 5 µM) to block NMDA and $GABA_A$ receptors, respectively. Input-output function of EPSCs was studied by delivering current pulses of incremental intensity (0–600µA, 50µA steps); 10 trials per pulse intensity were delivered and responses averaged to determine EPSC amplitude (initial EPSC peak). The slope (synaptic gain) and *x*-intercept (minimal stimulation intensity) of the linear regression of the input-output relationship were measured on averaged responses of individual cells. Spontaneous EPSCs were recorded over a period of 5 min and generally 300 consecutive events were analyzed (except for some cells with low frequency of events: TBS_{opto} group 4 cells with 168, 188, 200 and 261 events; no TBS_{opto} group 2 cells with 279 and 294 event) for frequency and amplitude (Clampfit 10.7).

EPSPs evoked by focal optogenetic stimulation through the objective were elicited using a Polygon400 Multiwavelength Dynamic Patterned Illuminator (Mightex). An area (20x20 to 20x30 µm) lateral to the recorded cell soma was illuminated with brief pulses of blue light (470 nm; duration 0.5-2 ms). EPSPs evoked by whole field optogenetic stimulation were elicited using a 4-Channel LED Driver (DC4104; Thorlabs) coupled to an optical fiber (MF79L01; 400 µm core diameter, 0.39 NA; Thorlabs) and fiber optic cannula (CFM14L20; 400 µm core diameter, 0.39 NA; Thorlabs) positioned above the CA1 stratum oriens region of the slice with brief light pulses (470 nm; duration 0.5-2 ms). In some experiments, the mGluR1a antagonist LY367385 (40 µM) was added in the ACSF during recordings. In other experiments, slices were pre-incubated in ACSF with 2 µM of the irreversible transcription inhibitor actinomycin D for 15 min prior to recording (Yuan and Burrell, 2013, Younts et al., 2016).

LTP induction protocol during whole cell current clamp recording

Test EPSPs were evoked at 0.1Hz. LTP induced by electrical stimulation was elicited by theta burst stimulation (TBS) consisting of 3 episodes (given at 30 s intervals) of 5 bursts (at 250 ms interburst intervals) of 4 electrical pulses at 100 Hz (Vasuta et al., 2015). LTP induced by optogenetic stimulation of CA1 pyramidal cells (TBS_{opto}) was elicited by TBS consisting of 3 episodes (given at 30 s intervals) of 5 bursts (at 300 ms inter-burst interval) of 4 light pulses at 80 Hz. In some experiments, low frequency optogenetic stimulation (LFS_{opto}) was given as 3 episodes (given at 30 s intervals) of 3 bursts (at 500 ms inter-burst interval) of 3 light pulses at 20 Hz. Test EPSP amplitude was averaged in 2 minutes bins before and after LTP induction. EPSPs were characterized in one cell per slice, and responses were analyzed off-line using Clampfit (pClamp 10.5/10.6; Molecular Devices) and GraphPad Prism 6.

Field potential recording

For experiments with field potential recordings, transverse hippocampal slices were prepared as described above, except oxygenated ACSF contained 1.3 mM $MgSO_4$ and 2.5 mM $CaCl_2$. The slices were let to recover for at least 2 h at 32°C in ACSF, and for an additional 30 minutes at 27°–28°C while submerged in a recording chamber continuously perfused (2–2.5 ml/min) with ACSF. Extracellular field EPSPs were recorded with borosilicate glass pipettes (3–4MΩ) filled with ACSF using a differential extracellular amplifier (Microelectrode AC Amplifier Model 1800, A-M Systems), filtered at 2 kHz, digitized at 10 kHz (Digidata 1440A), and analyzed with pClamp10.5. For Schaffer collateral-evoked fEPSPs, the concentric bipolar tungsten stimulating electrode (FHC) and recording pipette were placed in stratum radiatum. For temporo-ammonic pathway evoked fEPSPs, the stimulation and recording electrodes were positioned in stratum lacunosum-moleculare. Stimulus (0.1 ms duration; 15 sec^{-1}) strength was adjusted to elicit 50% of

maximal fEPSP and fEPSP slope was measured at 10–90% of fEPSP amplitude. CA1 pyramidal cell long-term potentiation was induced by weak theta burst stimulation (wTBS; 2 bursts of 4 pulses at 100 Hz, with 200 ms inter-burst interval) (Leao et al., 2012). Optogenetic induction of LTP in SOM interneurons was elicited as described above through a fiber optic positioned above the CA1 stratum oriens/alveus region of the slice.

Optogenetic stimulation in vivo

One week after viral injections, mice were anesthetised using ketamine and xylazine as described above, and fiber cannulas were stereotaxically implanted bilaterally (coordinates relative to bregma: -1.95 AP; ±1.60 ML; and -1.15 DV) and sealed with dental cement (Metabond, Parkell Inc). Animals were housed singly after the optic fiber implantation and allowed to rest for a week before behavioral experimentation. For in vivo optogenetic stimulation, a Quadruple Laser Diode Fiber Light Source (LDFLS_405/100_450/070_520/060_638/080; Doric Lenses Inc) was coupled to Mono Fiberoptic Patchcords (MFP_200/240/900-0.22_2m_FC-ZF1.25(F), 200 µm Core diameter, 0.22 NA; Doric Lenses Inc) and hand-made fiber optic cannulas (optic fiber: FT200EMT, 200 µm Core diameter, 0.22 NA; ceramic ferrule: CFLC230-10; Thorlabs).

Behavioral experiments

For all behavioral experiments, the experimenter was blind to the experimental groups (opsin *versus* reporter) from the day habituation began until data analysis was completed.

Habituation. Mice were gently handled daily for 5 days (5min/day) to progressively habituate them to the experimenter and reduce the stress related to the experimental handling and optic fiber connection (without light stimulation).

Open field test. Mice were allowed to freely explore a square arena (45 x 45 cm: Pan-Lab) for 15 min for the Arch experiments and 5 min for the hChR2 experiments. The anxiety level was assessed by measuring the time spent and the distance travelled in the center (1/3 central zone) of the arena compared to the periphery (1/3 peripheral zone). Locomotion was evaluated by measuring the total distance traveled and the number of zone transitions (16 equal squared zones). Mice were first video-tracked at 25 frames/s and their movements subsequently analyzed using a position tracking system (Smart 3.0; PanLab). For the Arch experiments, mice received continuous light stimulation (520 nm) for the 5-10 min period.

Contextual fear conditioning. Mice were trained in conditioning chambers that were housed in sound- and light-isolated cubicles (Coulbourn Instruments). The chambers contained a stainless-steel grid floor, overhead LED lighting, camera and were supplied with background noise (60 dB) by an air extractor fan. The experimental protocol was based on Lovett-Baron and coworkers (Lovett-Barron et al., 2014) with slight modifications. The training context was rectangular with 2 transparent and 2 stainless steel walls, was cleaned with 70% ethanol solution before and after each trial, and ethanol solution was added under the grid floor as a contextual smell. After 2 min free exploration, the animals received a weak fear conditioning consisting of 2 presentations of unconditioned stimulus (2 sec foot shock, 0.8mA; separated by 60 sec). To test for long-term contextual fear memory, the mice were returned to the training context during a test period of 3 min, at 24 h after conditioning. The freezing behavior was assessed using FreezeFrame (Coulbourn Instruments).

For the Arch optogenetic experiments, mice received light stimulation (520 nm; 6 sec pulses) in phase (starting 2 sec before) or shifted (30 sec before) relative to foot shocks during conditioning. For the TBS optogenetic experiments, mice were brought in the testing room on the

training day and, in their home cage, given the optogenetic TBS protocol (473 nm; 5 bursts of 4 light pulses of 1ms duration at 80 Hz, given at 300 ms interburst interval, and repeated 3 times with 30 s interval) or no light stimulation, 30 min prior to contextual fear conditioning.

Histology

Following *in vivo* optogenetic experiments, mice were deeply anesthetized intraperitoneally with sodium pentobarbital (MTC Pharmaceuticals), perfused transcardially first with 0.1M phosphate buffer saline (PBS) and next with 4% paraformaldehyde in 0.1M PBS (PFA). Brains were isolated, postfixed in 4% PFA for 24 hours and cryoprotected in 30% sucrose. Coronal brain sections (50 µm thick) were obtained using freezing microtome (SM200R; Leica) and mounted in ProLong Gold (Invitrogen). Sections were examined using an epifluorescence microscope (Eclipse E600; Nikon) and images were acquired with the Simple PCI software. Immunofluorescence was used to enhance GFP fluorescence associated with Arch. For these mice, brain sections were obtained as described above, permeabilized with 0.5% Triton X-100 in PBS for 15 minutes, and unspecific binding was blocked with 10% normal goat serum in 0.1% Triton X-100/PBS for 1 hour. Rabbit polyclonal GFP (1/200) antibodies were incubated for 48 hours at 4°C. Sections were subsequently incubated at room temperature with Alexa Fluor 594-conjugated goat anti-rabbit IgG (1/500; 90 min), mounted in ProLong Gold, and imaged as described above. For behavioral experiments, data were excluded if mice did not show virus expression restricted to CA1, and if optic fibers placement was outside the CA1 hippocampus.

Quantification and statistical analysis

No statistical methods were used to predetermine the sample size, but our sample sizes are similar to those used in the field. Statistical analysis was performed using SigmaPlot or GraphPad Prism 6 and 9. Data were tested for normality using the Shapiro–Wilk, D'Agostino and Pearson, Kolmogorov-Smirnov, and Brown–Forsythe tests. We used Student's *t* tests (with Welch corrections for heteroscedasticity), one- or two-way ANOVA, and one- or two-way mixed repeated-measures ANOVA, with Tukey's pairwise comparison tests (with Bonferroni adjustments for multiple comparisons) or with Holm-Sidak pairwise comparison tests when data passed normality and homoscedasticity assumptions. Mann–Whitney Rank Sum tests and Kruskal-Wallis one-way ANOVA on Ranks with Dunn's pairwise comparisons were used when it was not the case. All the tests were two-sided. All data in the Figures are presented as mean ± SEM. Asterisks in Figures denote statistical significance levels for specified tests (* $p < 0.05$; ** $p < 0.01$; *** $p < 0.001$; ns, not significant). Detailed results of all statistical tests referenced per Figure panel are given in Supplemental Table 1.

ACKNOWLEDGMENTS

This work was supported by grants to J.C.L. from the Canadian Institutes of Health Research (CIHR MOP-125985 and PJT-153311) and a Research Centre grant (Centre Interdisciplinaire de Recherche sur le Cerveau et l'Apprentissage; CIRCA) from the Fonds de la Recherche du Québec – Santé (FRQS). J.C.L. is the recipient of the Canada Research Chair in Cellular and Molecular Neurophysiology (CRC 950-231066) and a member of the Research Group on Neural Signaling and Circuitry (GRSNC) at Université de Montréal.

AUTHOR CONTRIBUTIONS

Conceptualization, J.C.L., A.A. and E.H.; Methodology, A.A., E.H and I.L.; Software, E.H.; Investigation, A.A., E.H., I.L. and F.X.M.; Writing – Original Draft, J.C.L., A.A., E.H. and I.L.; Writing – Review & Editing, J.C.L., A.A. and E.H.; Visualization, A.A., E.H. and I.L.; Supervision, Project Administration, and Funding Acquisition, J.C.L.

DECLARATION OF INTERESTS

The authors declare no competing interests.

REFERENCES

ARTINIAN, J., JORDAN, A., KHLAIFIA, A., HONORE, E., LA FONTAINE, A., RACINE, A. S., LAPLANTE, I. & LACAILLE, J. C. 2019. Regulation of Hippocampal Memory by mTORC1 in Somatostatin Interneurons. *J Neurosci,* 39**,** 8439-8456.

BANKO, J. L., HOU, L., POULIN, F., SONENBERG, N. & KLANN, E. 2006. Regulation of eukaryotic initiation factor 4E by converging signaling pathways during metabotropic glutamate receptor-dependent long-term depression. *J Neurosci,* 26**,** 2167-73.

BARTOS, M., ALLE, H. & VIDA, I. 2011. Role of microcircuit structure and input integration in hippocampal interneuron recruitment and plasticity. *Neuropharmacology,* 60**,** 730-9.

BLISS, T. V. & LOMO, T. 1973. Long-lasting potentiation of synaptic transmission in the dentate area of the anaesthetized rabbit following stimulation of the perforant path. *J Physiol,* 232**,** 331-56.

BOOKER, S. A., HARADA, H., ELGUETA, C., BANK, J., BARTOS, M., KULIK, A. & VIDA, I. 2020. Presynaptic GABAB receptors functionally uncouple somatostatin interneurons from the active hippocampal network. *Elife,* 9.

BOOKER, S. A., LORETH, D., GEE, A. L., WATANABE, M., KIND, P. C., WYLLIE, D. J. A., KULIK, A. & VIDA, I. 2018. Postsynaptic GABABRs Inhibit L-Type Calcium Channels and Abolish Long-Term Potentiation in Hippocampal Somatostatin Interneurons. *Cell Rep,* 22**,** 36-43.

BOOKER, S. A. & VIDA, I. 2018. Morphological diversity and connectivity of hippocampal interneurons. *Cell Tissue Res,* 373**,** 619-641.

CARDIN, J. A., CARLEN, M., MELETIS, K., KNOBLICH, U., ZHANG, F., DEISSEROTH, K., TSAI, L. H. & MOORE, C. I. 2010. Targeted optogenetic stimulation and recording of neurons in vivo using cell-type-specific expression of Channelrhodopsin-2. *Nat Protoc,* 5**,** 247-54.

CHIU, C. Q., MARTENSON, J. S., YAMAZAKI, M., NATSUME, R., SAKIMURA, K., TOMITA, S., TAVALIN, S. J. & HIGLEY, M. J. 2018. Input-Specific NMDAR-Dependent Potentiation of Dendritic GABAergic Inhibition. *Neuron,* 97**,** 368-377 e3.

CHOI, J. H., SIM, S. E., KIM, J. I., CHOI, D. I., OH, J., YE, S., LEE, J., KIM, T., KO, H. G., LIM, C. S. & KAANG, B. K. 2018. Interregional synaptic maps among engram cells underlie memory formation. *Science,* 360**,** 430-435.

COSTA-MATTIOLI, M., SOSSIN, W. S., KLANN, E. & SONENBERG, N. 2009. Translational control of long-lasting synaptic plasticity and memory. *Neuron,* 61**,** 10-26.

CROCE, A., PELLETIER, J. G., TARTAS, M. & LACAILLE, J. C. 2010. Afferent-specific properties of interneuron synapses underlie selective long-term regulation of feedback inhibitory circuits in CA1 hippocampus. *J Physiol,* 588**,** 2091-107.

FUHRMANN, F., JUSTUS, D., SOSULINA, L., KANEKO, H., BEUTEL, T., FRIEDRICHS, D., SCHOCH, S., SCHWARZ, M. K., FUHRMANN, M. & REMY, S. 2015. Locomotion, Theta Oscillations, and the Speed-Correlated Firing of Hippocampal Neurons Are Controlled by a Medial Septal Glutamatergic Circuit. *Neuron,* 86**,** 1253-64.

HIPPENMEYER, S., VRIESELING, E., SIGRIST, M., PORTMANN, T., LAENGLE, C., LADLE, D. R. & ARBER, S. 2005. A developmental switch in the response of DRG neurons to ETS transcription factor signaling. *PLoS Biol,* 3**,** e159.

HONORE, E., KHLAIFIA, A., BOSSON, A. & LACAILLE, J. C. 2021. Hippocampal Somatostatin Interneurons, Long-Term Synaptic Plasticity and Memory. *Front Neural Circuits,* 15**,** 687558.

HUANG, Y. H., SINHA, S. R., TANAKA, K., ROTHSTEIN, J. D. & BERGLES, D. E. 2004. Astrocyte glutamate transporters regulate metabotropic glutamate receptor-mediated excitation of hippocampal interneurons. *J Neurosci,* 24**,** 4551-9.

HUBER, K. M., KAYSER, M. S. & BEAR, M. F. 2000. Role for rapid dendritic protein synthesis in hippocampal mGluR-dependent long-term depression. *Science,* 288**,** 1254-7.

JIANG, X., LUPIEN-MEILLEUR, A., TAZERART, S., LACHANCE, M., SAMAROVA, E., ARAYA, R., LACAILLE, J. C. & ROSSIGNOL, E. 2018. Remodeled cortical inhibition prevents motor seizures in generalized epilepsy. *Ann Neurol,* 84**,** 436-451.

KATONA, L., LAPRAY, D., VINEY, T. J., OULHAJ, A., BORHEGYI, Z., MICKLEM, B. R., KLAUSBERGER, T. & SOMOGYI, P. 2014. Sleep and movement differentiates actions of two types of somatostatin-expressing GABAergic interneuron in rat hippocampus. *Neuron,* 82**,** 872-86.

KLAUSBERGER, T., MAGILL, P. J., MARTON, L. F., ROBERTS, J. D., COBDEN, P. M., BUZSAKI, G. & SOMOGYI, P. 2003. Brain-state- and cell-type-specific firing of hippocampal interneurons in vivo. *Nature,* 421**,** 844-8.

KLAUSBERGER, T. & SOMOGYI, P. 2008. Neuronal diversity and temporal dynamics: the unity of hippocampal circuit operations. *Science,* 321**,** 53-7.

KULLMANN, D. M., MOREAU, A. W., BAKIRI, Y. & NICHOLSON, E. 2012. Plasticity of inhibition. *Neuron,* 75**,** 951-62.

LAMSA, K. P., HEEROMA, J. H., SOMOGYI, P., RUSAKOV, D. A. & KULLMANN, D. M. 2007. Anti-Hebbian long-term potentiation in the hippocampal feedback inhibitory circuit. *Science,* 315**,** 1262-6.

LAPOINTE, V., MORIN, F., RATTE, S., CROCE, A., CONQUET, F. & LACAILLE, J. C. 2004. Synapse-specific mGluR1-dependent long-term potentiation in interneurones regulates mouse hippocampal inhibition. *J Physiol,* 555**,** 125-35.

LEAO, R. N., MIKULOVIC, S., LEAO, K. E., MUNGUBA, H., GEZELIUS, H., ENJIN, A., PATRA, K., ERIKSSON, A., LOEW, L. M., TORT, A. B. & KULLANDER, K. 2012. OLM interneurons differentially modulate CA3 and entorhinal inputs to hippocampal CA1 neurons. *Nat Neurosci,* 15**,** 1524-30.

LOVETT-BARRON, M., KAIFOSH, P., KHEIRBEK, M. A., DANIELSON, N., ZAREMBA, J. D., REARDON, T. R., TURI, G. F., HEN, R., ZEMELMAN, B. V. & LOSONCZY, A. 2014. Dendritic inhibition in the hippocampus supports fear learning. *Science,* 343**,** 857-63.

LOVETT-BARRON, M., TURI, G. F., KAIFOSH, P., LEE, P. H., BOLZE, F., SUN, X. H., NICOUD, J. F., ZEMELMAN, B. V., STERNSON, S. M. & LOSONCZY, A. 2012. Regulation of neuronal input transformations by tunable dendritic inhibition. *Nat Neurosci,* 15**,** 423-30, S1-3.

MADISEN, L., ZWINGMAN, T. A., SUNKIN, S. M., OH, S. W., ZARIWALA, H. A., GU, H., NG, L. L., PALMITER, R. D., HAWRYLYCZ, M. J., JONES, A. R., LEIN, E. S. & ZENG, H. 2010. A robust and high-throughput Cre reporting and characterization system for the whole mouse brain. *Nat Neurosci,* 13**,** 133-40.

MCBAIN, C. J. & KAUER, J. A. 2009. Presynaptic plasticity: targeted control of inhibitory networks. *Curr Opin Neurobiol,* 19**,** 254-62.

MCKAY, B. M., OH, M. M. & DISTERHOFT, J. F. 2013. Learning increases intrinsic excitability of hippocampal interneurons. *J Neurosci,* 33**,** 5499-506.

MULLER, C. & REMY, S. 2014. Dendritic inhibition mediated by O-LM and bistratified interneurons in the hippocampus. *Front Synaptic Neurosci,* 6**,** 23.

NABAVI, S., FOX, R., PROULX, C. D., LIN, J. Y., TSIEN, R. Y. & MALINOW, R. 2014. Engineering a memory with LTD and LTP. *Nature,* 511**,** 348-52.

NICHOLSON, E. & KULLMANN, D. M. 2021. Nicotinic receptor activation induces NMDA receptor independent long-term potentiation of glutamatergic signalling in hippocampal oriens interneurons. *J Physiol,* 599**,** 667-676.

OLESKEVICH, S., DESCARRIES, L. & LACAILLE, J. C. 1989. Quantified distribution of the noradrenaline innervation in the hippocampus of adult rat. *J Neurosci,* 9**,** 3803-15.

PELKEY, K. A., CHITTAJALLU, R., CRAIG, M. T., TRICOIRE, L., WESTER, J. C. & MCBAIN, C. J. 2017. Hippocampal GABAergic Inhibitory Interneurons. *Physiol Rev,* 97**,** 1619-1747.

PELLETIER, J. G. & LACAILLE, J. C. 2008. Long-term synaptic plasticity in hippocampal feedback inhibitory networks. *Prog Brain Res,* 169**,** 241-50.

PEREZ, Y., MORIN, F. & LACAILLE, J. C. 2001. A hebbian form of long-term potentiation dependent on mGluR1a in hippocampal inhibitory interneurons. *Proc Natl Acad Sci U S A,* 98**,** 9401-6.

POUILLE, F. & SCANZIANI, M. 2004. Routing of spike series by dynamic circuits in the hippocampus. *Nature,* 429**,** 717-23.

RAN, I., LAPLANTE, I., BOURGEOIS, C., PEPIN, J., LACAILLE, P., COSTA-MATTIOLI, M., PELLETIER, J., SONENBERG, N. & LACAILLE, J. C. 2009. Persistent transcription- and translation-dependent long-term potentiation induced by mGluR1 in hippocampal interneurons. *J Neurosci,* 29**,** 5605-15.

ROYER, S., ZEMELMAN, B. V., LOSONCZY, A., KIM, J., CHANCE, F., MAGEE, J. C. & BUZSAKI, G. 2012. Control of timing, rate and bursts of hippocampal place cells by dendritic and somatic inhibition. *Nat Neurosci,* 15**,** 769-75.

SENGUPTA, S., PETERSON, T. R., LAPLANTE, M., OH, S. & SABATINI, D. M. 2010. mTORC1 controls fasting-induced ketogenesis and its modulation by ageing. *Nature,* 468**,** 1100-4.

SHARMA, V., SOOD, R., KHLAIFIA, A., ESLAMIZADE, M. J., HUNG, T. Y., LOU, D., ASGARIHAFSHEJANI, A., LALZAR, M., KINIRY, S. J., STOKES, M. P., COHEN, N., NELSON, A. J., ABELL, K., POSSEMATO, A. P., GAL-BEN-ARI, S., TRUONG, V. T., WANG, P., YIANNAKAS, A., SAFFARZADEH, F., CUELLO, A. C., NADER, K., KAUFMAN, R. J., COSTA-MATTIOLI, M., BARANOV, P. V., QUINTANA, A., SANZ, E., KHOUTORSKY, A., LACAILLE, J. C., ROSENBLUM, K. & SONENBERG, N. 2020. eIF2alpha controls memory consolidation via excitatory and somatostatin neurons. *Nature,* 586**,** 412-416.

SUN, Y., NGUYEN, A. Q., NGUYEN, J. P., LE, L., SAUR, D., CHOI, J., CALLAWAY, E. M. & XU, X. 2014. Cell-type-specific circuit connectivity of hippocampal CA1 revealed through Cre-dependent rabies tracing. *Cell Rep,* 7**,** 269-80.

SZONYI, A., SOS, K. E., NYILAS, R., SCHLINGLOFF, D., DOMONKOS, A., TAKACS, V. T., POSFAI, B., HEGEDUS, P., PRIESTLEY, J. B., GUNDLACH, A. L., GULYAS, A. I., VARGA, V., LOSONCZY, A., FREUND, T. F. & NYIRI, G. 2019. Brainstem nucleus incertus controls contextual memory formation. *Science,* 364.

TANIGUCHI, H., HE, M., WU, P., KIM, S., PAIK, R., SUGINO, K., KVITSIANI, D., FU, Y., LU, J., LIN, Y., MIYOSHI, G., SHIMA, Y., FISHELL, G., NELSON, S. B. & HUANG, Z. J. 2011. A resource of Cre driver lines for genetic targeting of GABAergic neurons in cerebral cortex. *Neuron,* 71**,** 995-1013.

TYAN, L., CHAMBERLAND, S., MAGNIN, E., CAMIRE, O., FRANCAVILLA, R., DAVID, L. S., DEISSEROTH, K. & TOPOLNIK, L. 2014. Dendritic inhibition provided by interneuron-specific cells controls the firing rate and timing of the hippocampal feedback inhibitory circuitry. *J Neurosci,* 34**,** 4534-47.

UDAKIS, M., PEDROSA, V., CHAMBERLAIN, S. E. L., CLOPATH, C. & MELLOR, J. R. 2020. Interneuron-specific plasticity at parvalbumin and somatostatin inhibitory synapses onto CA1 pyramidal neurons shapes hippocampal output. *Nat Commun,* 11**,** 4395.

VASUTA, C., ARTINIAN, J., LAPLANTE, I., HEBERT-SEROPIAN, S., ELAYOUBI, K. & LACAILLE, J. C. 2015. Metaplastic Regulation of CA1 Schaffer Collateral Pathway Plasticity by Hebbian MGluR1a-Mediated Plasticity at Excitatory Synapses onto Somatostatin-Expressing Interneurons. *eNeuro,* 2.

YOUNTS, T. J., MONDAY, H. R., DUDOK, B., KLEIN, M. E., JORDAN, B. A., KATONA, I. & CASTILLO, P. E. 2016. Presynaptic Protein Synthesis Is Required for Long-Term Plasticity of GABA Release. *Neuron,* 92**,** 479-492.

YUAN, S. & BURRELL, B. D. 2013. Endocannabinoid-dependent long-term depression in a nociceptive synapse requires coordinated presynaptic and postsynaptic transcription and translation. *J Neurosci,* 33**,** 4349-58.

Figure 1–figure supplement 1

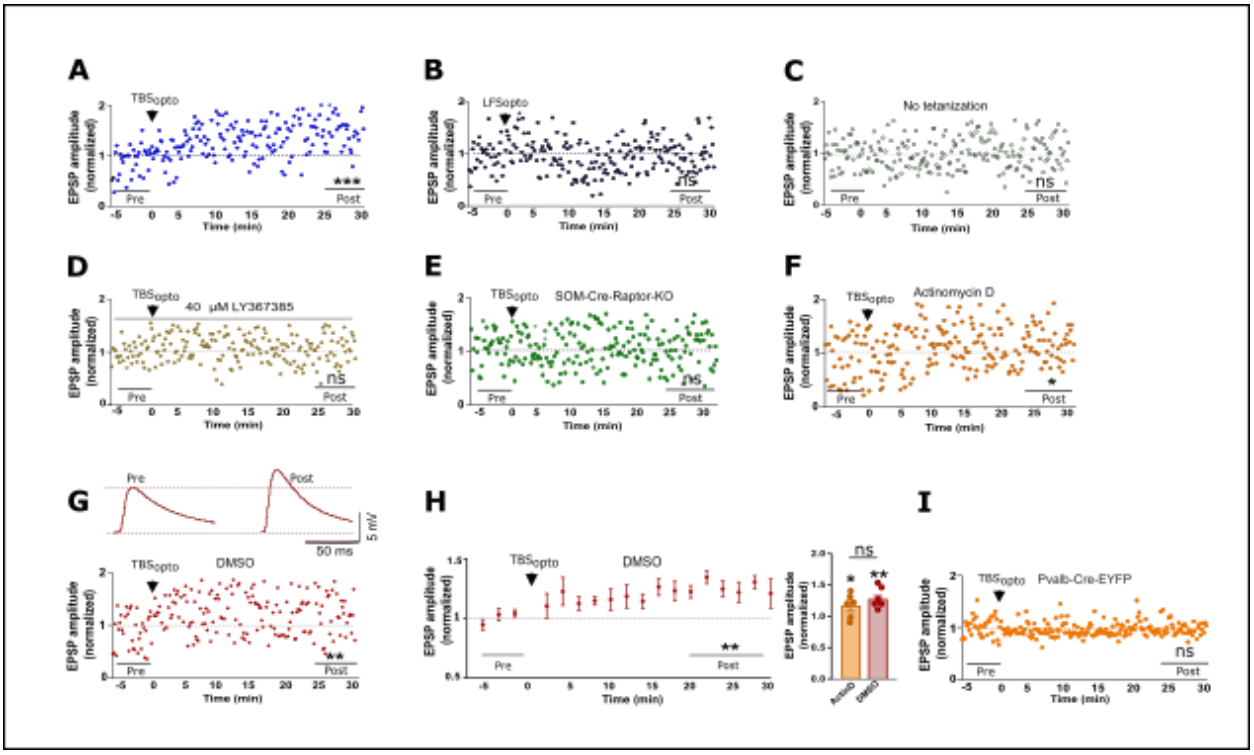

Figure S1 (Related to Figure 1). Optogenetically-induced LTP at PC-SOM synapses in representative cells. (A to E) Time plots of light-evoked EPSP amplitude from representative SOM cells (EPSPs shown in Figure 1B to 1G) showing LTP at PC-SOM synapses after TBS_{opto} (A), but not after LFS_{opto} (B), no tetanization (C), TBS_{opto} in LY367385 (D), or TBS_{opto} in SOM-Cre-Raptor-KO mice (E). Paired t-tests at 25-30 min after induction (Post) relative to baseline (Pre), *** $p < 0.0001$, ns $p > 0.05$. (F and G) Time plots of light-evoked EPSP amplitude from representative SOM cells (EPSPs shown in Figure 1G for cell in F), showing LTP at PC-SOM synapses after TBS_{opto} after incubation with the transcription inhibitor actinomycin D (F) or its vehicle DMSO (G; EPSPs above). Paired t-tests, * $p < 0.05$, ** $p < 0.01$. (H) Left: time plot of light-evoked EPSP amplitude for all SOM cells tested showing LTP at PC-SOM synapses following TBS_{opto} after incubation with DMSO (n = 6 cells). Right: Summary graph of EPSP amplitude for all cells at 20-30 min post induction, showing similar LTP after TBS_{opto} after incubation in actinomycin D or its vehicle DMSO. Paired t-tests (Pre vs Post) and unpaired t-test (Post Actin D vs Post DMSO), * $p < 0.05$, ** $p < 0.01$, ns $p>0.05$. (I) Time plots of light-evoked EPSP amplitude from representative Pvalb cell (EPSPs shown in Figure 1I) showing absence of LTP at PC-Pvalb synapses after TBS_{opto}. Paired t-test, ns $p>0.05$.

Figure 1–figure supplement 2

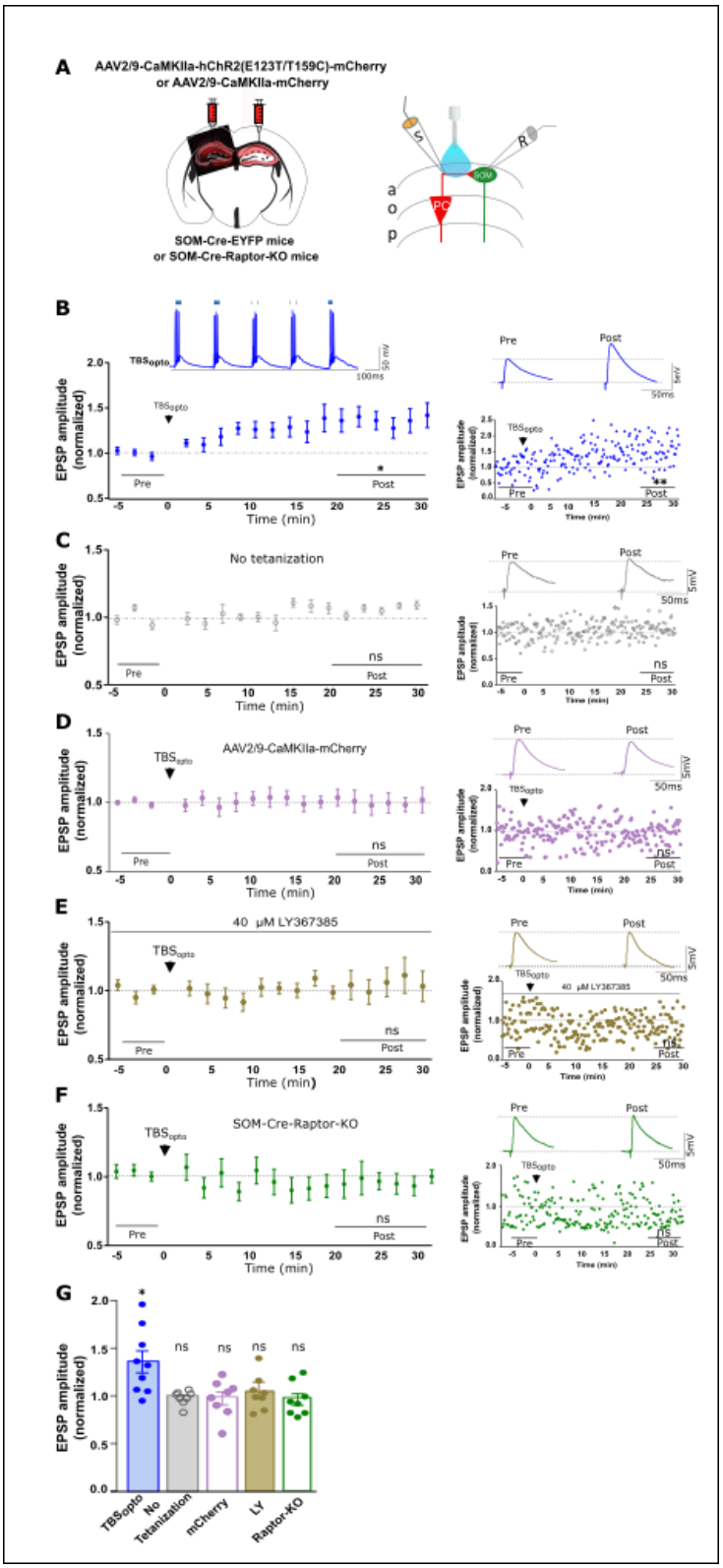

Figure S2 (Related to Figure 1). Optogenetically-induced LTP of electrically-evoked EPSPs in SOM cells. (A) Left: schematic of experimental paradigm with viral injections in dorsal hippocampus of SOM-Cre-EYFP or SOM-Cre-Raptor-KO mice. Right: diagram of local optogenetic stimulation of CA1 pyramidal cells, electrical stimulation of afferents and whole cell recording from SOM cells. (B) Left: time plot of electrically-evoked EPSP amplitude for all SOM cells, showing LTP at 20-30 min following TBS_{opto} (n = 9 cells). Inset above: EPSP summation and cell firing during TBS_{opto}. Right: example of EPSPs (top) and time plot (bottom) from a representative cell, before (Pre) and 25-30 min after (Post) induction. Paired t-tests; ** $p < 0.01$, * $p < 0.05$. (C - F) Time plots of electrically-evoked EPSP amplitude for all SOM cells (left) and example of EPSPs (top) and time plot (bottom) from a representative cell (right), showing absence of LTP of electrically-evoked EPSP amplitude following no tetanization (C; n = 8 cells), or following TBS_{opto} in slices from mice with control CaMKIIa-mCherry injection without hChR2 (D; n = 8 cells), TBS_{opto} in the presence of the mGluR1a antagonist LY367385 (40 µM) (E; n = 8 cells), or TBS_{opto} in SOM-Cre-Raptor-KO mice (F; n = 8 cells). Paired t-tests; ns, $p > 0.05$. (G) Summary graph of EPSP amplitude for all cells at 20-30 min post induction, showing LTP after TBS_{opto}, but no LTP in absence of tetanization, or after TBS_{opto} in mice injected with mCherry, in LY367385, or in SOM-Cre-Raptor-KO mice. Paired t-tests (Pre vs Post); * $p < 0.05$, ns $p > 0.05$.

Figure 2–figure supplement 1

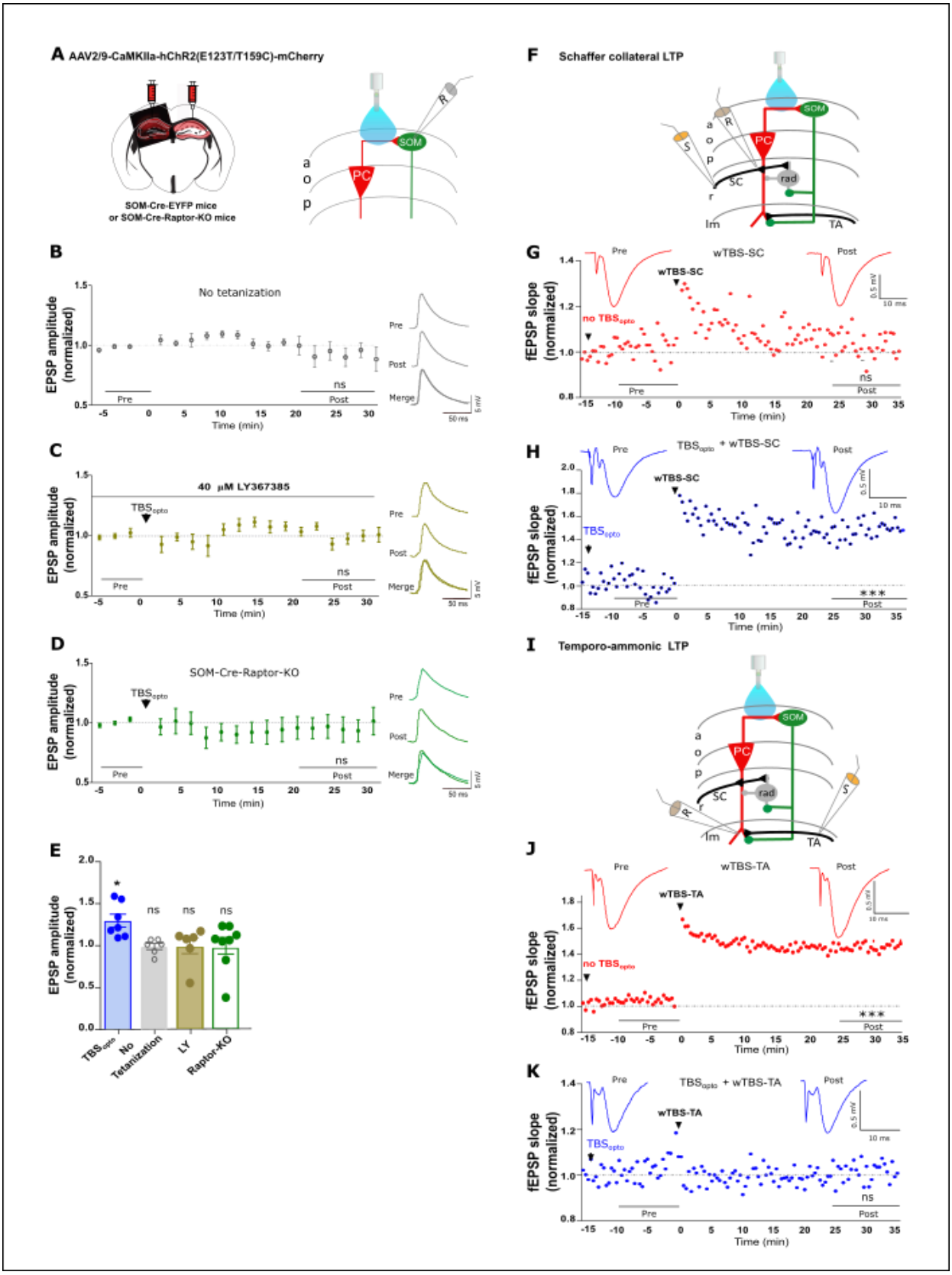

Figure S3 (related to Figure 2). Whole-field TBS_{opto}-induced LTP at PC-SOM synapses and differential regulation of LTP at SC-PC and TA-PC synapses. (A) Left: schematic of experimental paradigm with viral injections in dorsal hippocampus of SOM-Cre-EYFP or SOM-Cre-Raptor-KO mice. Right: diagram of whole-field optogenetic stimulation of CA1 pyramidal cells and whole cell recording from SOM interneurons. (B-D) Left: time plots of light-evoked EPSP amplitude for all SOM cells, showing absence of LTP at PC-SOM synapses following no tetanization (B; n = 6 cells), TBS_{opto} in the presence of the mGluR1a antagonist LY367385 (C; n = 6 cells), or TBS_{opto} in SOM-Cre-Raptor-KO mice (D; n = 8 cells). Right: representative example of average EPSPs before (Pre) and 20-30 min after (Post) induction in each treatment condition. Paired t-tests, ns $p > 0.05$. (E) Summary graph of light-evoked EPSP amplitude for all cells at 20-30 min post induction, showing LTP after TBS_{opto}, but not in absence of tetanization, nor after TBS_{opto} in LY367385 or SOM-Cre-Raptor-KO mice. Paired t-tests; * $p < 0.05$, ns $p > 0.05$. (F) Diagram of whole-field optogenetic stimulation of CA1 pyramidal cells, with electrical stimulation and recording of SC-PC fEPSPs in stratum radiatum. (G-H) Time plots of fEPSP slope (with average fEPSPs above) from representative slices, showing that LTP at SC-PC synapses (G; red) is facilitated by prior application of TBS_{opto} (H; blue). Paired t-tests, *** $p < 0.001$, ns, $p > 0.05$. (I) Diagram of whole-field optogenetic stimulation of CA1 pyramidal cells, with electrical stimulation and recording of TA-PC fEPSPs in stratum lacunosum-moleculare. (J-K) Time plots of fEPSP slope (with average fEPSPs above) from representative slices, showing that LTP at TA-PC synapses (J; red) is depressed by prior application of TBS_{opto} (H; blue). Paired t-tests, *** $p < 0.001$, ns, $p > 0.05$.

Figure 3–figure supplement 1

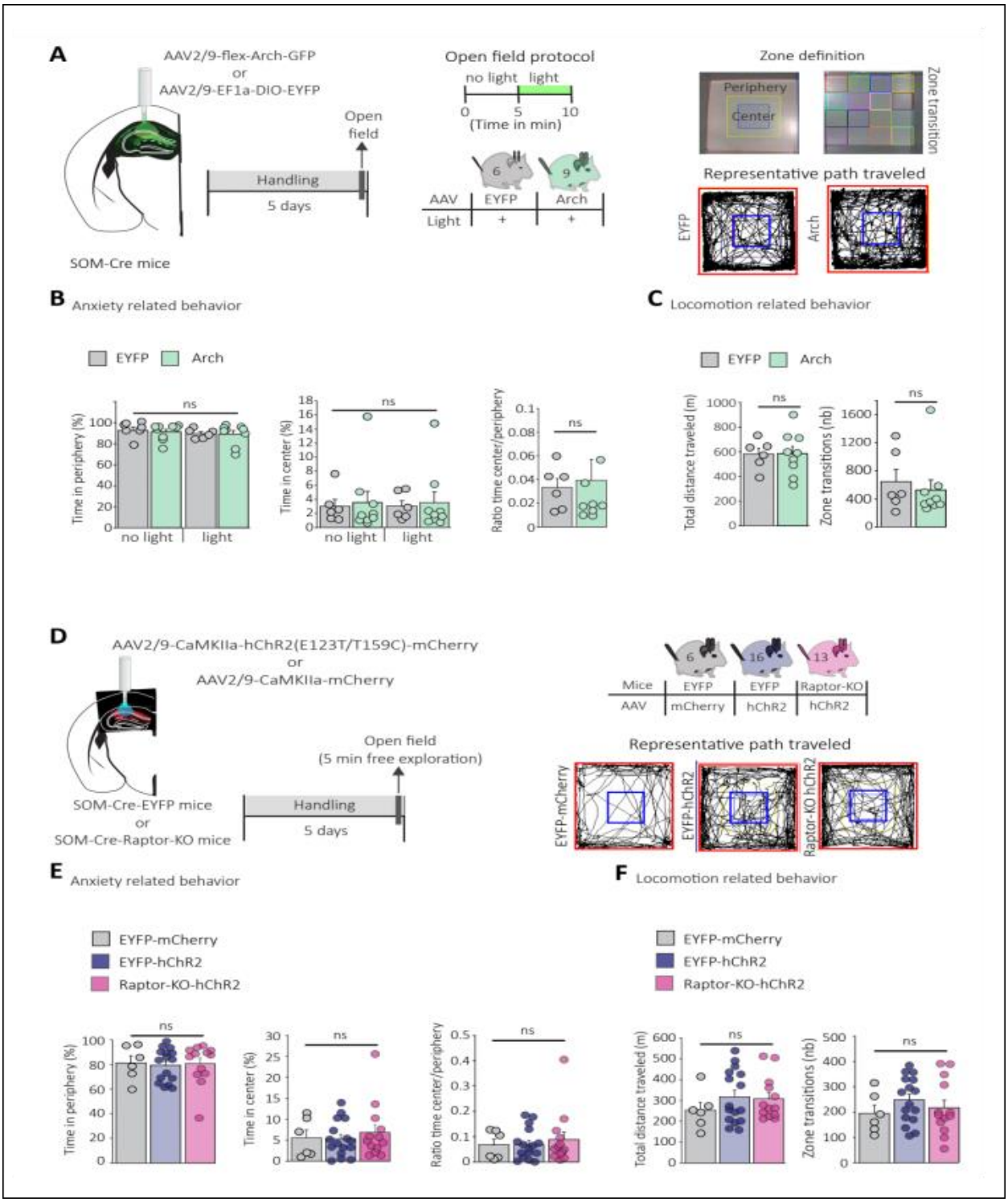

Figure S4 (related to Figure 3) Normal anxiety and locomotion in open-field tests. (A) Left: schematic of experimental paradigm with injections of AAV2/9-flex-Arch-GFP or AAV2/9-EF1a-DIO-EYFP in dorsal CA1 hippocampus of SOM-Cre mice. Middle: diagram of protocol during two open field test episodes, first without light and second with light for optogenetic silencing of SOM interneurons. Right: (top) zone separations used for analysis and (bottom) representative examples of path traveled by mice with EYFP (left) or Arch (right) expression in open field test.
(B) Summary graphs for all mice showing unchanged time spent in periphery (left) and center (middle), and ratio of time in center/periphery (right), of mice that received light activation of Arch (Arch; n=9 mice, green) relative to mice with light stimulation without Arch (EYFP; n=6 mice, grey) during open field tests without and with light, indicating normal anxiety level in both groups. Two-way repeated measures ANOVA (time spent in periphery and center); Mann-Whitney Rank Sum Test (ratio of time center/periphery); ns $p>0.05$. (C) Summary graphs for all mice showing unchanged total distance traveled and zone transitions in mice that received light activation of Arch (green) relative to mice with light stimulation without Arch (gray) during open field tests, indicating normal locomotion in both groups. Unpaired t-test (distance traveled) and Mann-Whitney Rank Sum Test (zone transitions), ns $p>0.05$. (D) Left: Schematic of experimental paradigm with injections of AAV2/9-CaMKIIa-hChR2(E123T/T159C)-mCherry or AAV2/9-CaMKIIa-mCherry in dorsal CA1 hippocampus of SOM-Cre-EYFP and SOM-Cre-Raptor-KO mice, and diagram of behavioral testing sequence (open field test). Right: representative examples of path traveled in open field test by SOM-Cre-EYFP mice with mCherry or hChR2 expression, and SOM-Cre-Raptor-KO mice with hChR2 expression. (E) Summary graphs for all mice showing unchanged time spent in periphery (left) and center (middle), and ratio of time in center/periphery (right), of SOM-Cre-EYFP mice with mCherry expression (n=6 mice, grey) or hChR2 expression (n=16 mice, violet), and SOM-Cre-Raptor-KO mice with hChR2 expression (n=13 mice, pink), indicating normal anxiety level. Kruskal-Wallis one-way ANOVA on Ranks, ns $p>0.05$.
(F) Summary graphs for all mice showing unchanged total distance traveled and zone transition number of SOM-Cre-EYFP mice with mCherry expression (n=6 mice, pink) or hChR2 expression (n=15 mice, blue), and SOM-Cre-Raptor-KO mice with hChR2 expression (n=13 mice, green), indicating normal locomotion. Kruskal-Wallis one-way ANOVA on Ranks (distance traveled), one-way ANOVA (zone transitions), ns $p>0.05$.

Table S1. Details of statistical comparisons. Related to Fig.1-4, S1-4.

Figure	Panel	Group size	Test	Statistic	P values	Statistic 2	P values 2
1	B	TBS_{opto} n=17	Paired t-test	t (16) =6.312	P < 0.0001		
1	C	LFS_{opto} n=8	Paired t-test	t (7) =0.449	P = 0.667		
1	D	No tetanization n=13	Paired t-test	t (12) =1.138	P=0.277		
1	E	LY n=10	Paired t-test	t (9) =2.141	P = 0.06		
1	F	SOM-Cre-Raptor-KO n=15	Paired t-test	t (14) =0.5457	P = 0.5939		
1	G	Actin D n=6	Paired t-test	t (5) =3.482	P = 0.0176		
1	I	Pvalb-Cre-EYFP n=8	Paired t-test	t (7) =1.578	P = 0.158		
1	J	TBS_{opto} n=17 LFS_{opto} n=8 No tetanization n=13 LY n=10 SOM-Cre-Raptor-KO n=15 Actin D n=6 Pvalb-Cre-EYFP n=8	Paired t-tests (as above, B-I)	as above, B-I	as above, B-I	Unpaired t-test, 20-30 min post induction, TBS_{opto} vs Actin D, t (21) =1.396	P= 0.1772
SUP1	A	TBS_{opto} Pre n=36 Post n=36	Paired t-test	t (35) =8.243	P<0.0001		
SUP1	B	LFS_{opto} Pre n=36 Post n=36	Paired t-test	t (35) =0.6396	P=0.5266		
SUP1	C	No tetanization Pre n=36 Post n=36	Paired t-test	t (35) =0.3376	P=0.7377		
SUP1	D	LY Pre n=36 Post n=36	Paired t-test	t (35) =0.7724	P=0.4450		
SUP1	E	SOM-Cre-Raptor-KO Pre n=36 Post n=36	Paired t-test	t (35) =0.3611	P=0.7202		
SUP1	F	Actin D Pre n=36 Post n=36	Paired t-test	t (35) =2.624	P=0.0128		
SUP1	G	DMSO Pre n=36 Post n=36	Paired t-test	t (35) =3.354	P=0.0019		

SUP1	H (left)	DMSO n=6	Paired t-test	t (5) =4.175	P = 0.0087		
SUP1	H (right)	Actin D n=6 DMSO n=6	Paired t-test, as above (Fig 1G and SUP 1H left)	Actin D t (5) =3.482 DMSO t (5) =4.175	Actin D P = 0.0176 DMSO P = 0.0087	Unpaired t-test, 20-30 min post induction, Actin D vs DMSO, t (10) =1.03	P= 0.3272
SUP1	I	Pvalb-Cre-EYFP Pre n=36 Post n=36	Paired t-test	t (35) =0.2349	P=0.8157		
SUP2	B left	TBS_{opto} n=9	Paired t-test	t (8) =3.248	P=0.0117		
SUP2	B right	TBS_{opto} Pre n=36 Post n=36	Paired t-test	t (35) =3.129	P=0.0035		
SUP2	C left	No tetanization n=8	Paired t-test	t (7) =1.198	P = 0.270		
SUP2	C right	No tetanization Pre n=36 Post n=36	Paired t-test	t (35) =1.346	P= 0.1871		
SUP2	D left	AAV9-CaMKIIa-mCherry n=8	Paired t-test	t (7) =0.04446	P = 0.965		
SUP2	D right	AAV9-CaMKIIa-mCherry Pre n=36 Post n=36	Paired t-test	t (35) =0.6835	P=0.4988		
SUP2	E left	LY n=8	Paired t-test	t (7) =1.058	P = 0.325		
SUP2	E right	LY Pre n=36 Post n=36	Paired t-test	t (35) =1.299	P=0.2026		
SUP2	F left	SOM-Cre-Raptor-KO n=8	Paired t-test	t (7) =0.3832	P = 0.712		
SUP2	F right	SOM-Cre-Raptor-KO Pre n=36 Post n=36	Paired t-test	t (35) =1.352	P=0.1850		
SUP2	G	TBS_{opto} n=9 No tetanization n=8 9-CaMKIIa-mCherry n=8 LY n=8 SOM-Cre-Raptor-KO n=8	Paired t-tests (as above, B-F left)	as above, B-F left	as above, B-F left		
SUP3	B	No tetanization n=6	Paired t-test	t (5) =0.6528	P = 0.542		
SUP3	C	LY n=6	Paired t-test	t (5) =0.3449	P = 0.744		
SUP3	D	SOM-Cre-Raptor-KO n=8	Paired t-test	t (7) =0.4145	P = 0.690		

SUP3	E	TBS_{opto} n=7 No tetanization n=6 LY n=6 SOM-Cre-Raptor-KO n=8	Paired t-tests (as above, B-D; and Fig 2B below)	as above, B-D; and Fig 2B below	as above, B-D; and Fig 2B below		
SUP3	G	wTBS-SC Pre n=24 Post n=24	Paired t-test	t (24) = 0.3405	P = 0.7365		
SUP3	H	TBS_{opto}+wTBS-SC Pre n=24 Post n=24	Paired t-test	t (24) =22.14	P <0.0001		
SUP3	J	wTBS-TA Pre n=24 Post n=24	Paired t-test	t (24) =60.20	P <0.0001		
SUP3	K	TBS_{opto}+wTBS-TA Pre n=24 Post n=24	Paired t-test	t (24) =0.7208	P = 0.4780		
2	B	TBS_{opto} n=7	Paired t-test	t (6) = 3.455	P = 0.0135		
2	D	wTBS-SC n=13 TBS_{opto}+wTBS-SC n=11 LY+TBS_{opto} +wTBS-SC n=7 TBS_{opto} mCherry n=11	Paired t-test Paired t-test Paired t-test Paired t-test	t (12) =1.183 t (10) =4.410 t (6)= 1.618 t (10)=0.4497	P=0.2596 P = 0.0013 P = 0.1568 P = 0.6625		
2	E	wTBS-SC Raptor-KO n=9 TBS_{opto} +wTBS-SC Raptor-KO n=10	Paired t-test Paired t-test	t (8) = 2.215 t (9) =1.350	P= 0.0576 P= 0.2243		
2	F	Left: wTBS-SC n=13 TBS_{opto}+wTBS n=11 LY+TBS_{opto} +wTBS-SC n=7 TBS_{opto}+wTBS-SC mCherry n=11 Right: wTBS-SC Raptor-KO n=9 TBS_{opto} +wTBS-SC Raptor-KO n=10	One-way ANOVA Multiple comparison	F (3, 38) = 6.053	P = 0.0018	Tukey's multiple comparisons test Unpaired t-test, 25-35 min post induction	25-35 min post induction TBS_{opto} + wTBS-SC vs. wTBS-SC P= 0.0067 TBS_{opto} + wTBS-SC vs. LY+TBS_{opto} + wTBS-SC P= 0.0359 TBS_{opto} + wTBS-SC vs. TBS_{opto}+wTBS-SC mCherry P= 0.0028 wTBS-SC vs. LY+TBS_{opto} + wTBS-SC P= 0.9993 wTBS-SC vs. TBS_{opto}+wTBS-SC mCherry P= 0.9645 wTBS-SC Raptor-KO vs. TBS_{opto} +wTBS-SC Raptor-KO P= 0.4222 t (17) =0.8225

2	H	wTBS-TA n=7 TBS_{opto}+wTBS-TA n=6 LY+TBS_{opto} +wTBS-TA n=7 TBS_{opto}+wTBS-TA mCherry n=7	Paired t-test Paired t-test Paired t-test Paired t-test	t (6) =2.985 t (5) =0.955 t (6) =4.022 t (6) =2.695	P = 0.0245 P = 0.3833 P = 0.0069 P = 0.0358		
2	I	wTBS-TA Raptor-KO n=8 TBS_{opto} +wTBS-TA Raptor-KO n=7	Paired t-test Paired t-test	t (7) =4.385 t (6) =3.660	P = 0.0032 P = 0.0106		
2	J	Left: wTBS-TA n=7 TBS_{opto}+wTBS n=6 LY+TBS_{opto} +wTBS-TA n=7 TBS_{opto}+wTBS-TA mCherry n=7 Right: wTBS-TA Raptor-KO n=8 TBS_{opto} +wTBS-TA Raptor-KO n=7	One-way ANOVA Multiple comparison	F (3, 23) = 3.667	P = 0.0270	Tukey's multiple comparisons test Unpaired t-test, 25-35 min post induction	25-35 min post induction TBS_{opto} + wTBS-TA vs. wTBS-TA P= 0.0420 TBS_{opto} + wTBS-TA vs. LY+TBS_{opto} + wTBS-TA P= 0.0289 TBS_{opto} + wTBS-TA vs. TBS_{opto}+wTBS-TA mCherry P= 0.0405 wTBS-TA vs. LY+TBS_{opto} + wTBS-TA P=0.999 wTBS-TA vs. TBS_{opto}+wTBS-TA mCherry P >0.9999 wTBS-TA Raptor-KO vs. TBS_{opto} +wTBS-TA Raptor-KO P= 0.5516 t(13)=0.6113
3	C	EYFP-Phase n=8 Arch-Phase n=9 Arch-Shifted n=7	One-way ANOVA	F=10.188	P < 0.001	Holm-Sidak multiple comparisons test	Arch-Phase vs EYFP-Phase t = 2.627, P = 0.016 Arch-Phase vs Arch-Shifted t = 4.463, P <0.001 EYFP-Phase vs Arch-Shifted t = 1.879, P = 0.074
3	F Left	SOM-Cre-EYFP mice TBS_{opto} hChR2 n=8 no TBS_{opto} hChR2 n=7 TBS_{opto} EYFP n=8	Kruskal-Wallis One-way ANOVA on Ranks	H = 17.626	P = 0.001	Dunn's multiple comparisons test	TBS_{opto} vs. no TBS_{opto} P=0.001 TBS_{opto} vs. TBS_{opto} no hChR2 P=0.001 No TBS_{opto} vs. TBS_{opto} no hChR2 P >0.05
3	F Right	SOM-Cre-Raptor-KO mice TBS_{opto} n=86 no TBS_{opto} n=7	Unpaired t-test	t =-0.653	P = 0.527		
SUP4	B (Left) Time spent in periphery	EYFP n=6 Arch n=9	Two-way repeated measure ANOVA	EYFP vs Arch F = 0.12 no light vs light F = 0.0207	EYFP vs Arch P = 0.734 no light vs light P = 0.888		

				EYFP/Arch vs no light/light F = 0.892	EYFP/Arch vs no light/light P = 0.362		
SUP4	B (middle) Time spent in center	EYFP n=6 Arch n=9	Two-way repeated measure ANOVA	EYFP vs Arch F = 0.0688 no light vs light F = 0.000023 EYFP/Arch vs no light/light F = 0.00168	EYFP vs Arch P = 0.797 no light vs light P = 0.996 EYFP/Arch vs no light/light P = 0.968		
SUP4	B (Right) Ratio of time in center/periphery	EYFP n=6 Arch n=9	Mann-Whitney Rank Sum Test	T = 54	P = 0.517		
SUP4	C Total distance traveled	EYFP n=6 Arch n=9	Unpaired t-test	T = -0.0335	P = 0.974		
SUP4	C Zone transitions	EYFP n=6 Arch n=9	Mann-Whitney Rank Sum Test	T = 54	P = 0.517		
SUP4	E (Left) Time spent in periphery	SOM-Cre-EYFP mice mCherry n=6 SOM-Cre-EYFP mice hChR2 n=16 SOM-Cre-Raptor-KO mice hChR2 n=13	Kruskal-Wallis One Way Analysis of Variance on Ranks	H = 0.44	P = 0.802		
SUP4	E (middle) Time spent in center	SOM-Cre-EYFP mice mCherry n=6 SOM-Cre-EYFP mice hChR2 n=16 SOM-Cre-Raptor-KO mice hChR2 n=13	Kruskal-Wallis One Way Analysis of Variance on Ranks	H = 0.284	P = 0.868		
SUP4	E (Right) Ratio of time in center/periphery	SOM-Cre-EYFP mice mCherry n=6 SOM-Cre-EYFP mice hChR2 n=16 SOM-Cre-Raptor-KO mice hChR2 n=13	Kruskal-Wallis One Way Analysis of Variance on Ranks	H = 0.0549	P = 0.973		
SUP4	F (Left) Total distance	SOM-Cre-EYFP mice mCherry n=6 SOM-Cre-EYFP mice hChR2 n=16 SOM-Cre-Raptor-KO mice hChR2 n=13	Kruskal-Wallis One Way Analysis of Variance on Ranks	H = 1.274	P = 0.529		
SUP4	F (Right) Zone transitions	SOM-Cre-EYFP mice mCherry n=6 SOM-Cre-EYFP mice hChR2 n=16 SOM-Cre-Raptor-KO mice hChR2	One-way ANOVA	F =0.781	P = 0.466		

		n=13					
4	B	Baseline TBS #1 TBS #2, n=8	rmANOVA	F (2, 14) = 22.41	P<0.0001	Tukey's multiple comparisons tests	Baseline vs. TBS #1 P= 0.0079 TBS #1 vs. TBS #2 P=0.0199
4	C	Baseline TBS_{opto} #1 TBS_{opto} #2, n=7	rmANOVA	F (2, 12) = 14.71	P=0.0006	Tukey's multiple comparisons test	Baseline vs. TBS_{opto} #1 P=0.0029 TBS_{opto} #1 vs. TBS_{opto} #2 P=0.7365
4	D	Baseline TBS_{opto} #1 TBS #2, n=8	rmANOVA	F (2, 14) = 9.137	P=0.0029	Tukey's multiple comparisons test	Baseline vs. TBS_{opto} #1 P=0.0180 TBS_{opto} #1 vs. TBS #2 P= 0.0031
4	E	Baseline TBS #1 TBS_{opto} #2, n=8	rmANOVA	F (2, 14) = 8.467	P=0.0039	Tukey's multiple comparisons test	Baseline vs. TBS #1 P=0.0290 TBS #1 vs. TBS_{opto} #2 P=0.5483
4	F	Baseline no TBS #1 TBS #2, n=10	rmANOVA	F (2, 18) = 24.33	P<0.0001	Tukey's multiple comparisons test	Baseline vs. no TBS #1 P=0.8039 No TBS #1 vs. TBS #2 P<0.0001
4	H sEPSC frequency	TBS_{opto} and CFC n=18 cells, 3 mice No TBS_{opto} and CFC n=17 cells, 4 mice	Mann-Whitney Rank Sum Test	t = 389	P = 0.006		
4	H sEPSC amplitude	TBS_{opto} and CFC n=18 cells, 3 mice No TBS_{opto} and CFC n=17 cells, 4 mice	Mann-Whitney Rank Sum Test	t =397	P = 0.003		
4	I Slope of EPSC I-O	TBS_{opto} and CFC n=17 cells, 3 mice No TBS_{opto} and CFC n=19 cells, 4 mice	Mann-Whitney Rank Sum Test	t = 221	P = 0.028		